4. Reactor Description

4.1 Summary Description

The Kansas State University (KSU) Nuclear Reactor Facility, operated by the Department of Mechanical and Nuclear Engineering, is located in Ward Hall on the campus in Manhattan, Kansas. The Department is also the home of the Tate Neutron Activation Analysis Laboratory. The TRIGA reactor was obtained through a 1958 grant from the United States Atomic Energy Commission and is operated under Nuclear Regulatory Commission License R-88 and the regulations of Chapter 1, Title 10, Code of Federal Regulations. Chartered functions of the Nuclear Reactor Facility are to serve as: 1) an educational facility for all students at KSU and nearby universities and colleges, 2) an irradiation facility for researchers at KSU and for others in the central United States, 3) a facility for training nuclear reactor operators, and 4) a demonstration facility to increase public understanding of nuclear energy and nuclear reactor systems.

The KSU TRIGA reactor is a water-moderated, water-cooled thermal reactor operated in an open pool and fueled with heterogeneous elements consisting of nominally 20 percent enriched uranium in a zirconium hydride matrix and clad with stainless steel. Principal experimental features of the KSU TRIGA Reactor Facility are:

- Central thimble
- Rotary specimen rack
- Thermalizing column with bulk shielding tank
- Thermal column with removable door
- Beam ports
  - Radial (2)
  - Piercing (fast neutron) (1)
  - Tangential (thermal neutron) (1)

The reactor was licensed in 1962 to operate at a steady-state thermal power of 100 kilowatts (kW). The reactor has been licensed since 1968 to operate at a steady-state thermal power of 250 kW and a pulsing maximum thermal power of 250 MW. Application is made concurrently with license renewal to operate at a maximum of 1,250 kW, with fuel loading to support 500 kW steady state thermal power and with pulsing to $3.00 reactivity insertion. All cooling is by natural convection. The 250-kW core consists of 81 fuel elements typically (at least 83 planned for the 1,250-kW core), each containing as much as 39 grams of ^{235}U. The reactor core is in the form of a right circular cylinder about 23 cm (approximately 9 in.) radius and 38 cm (14.96 in.) depth, positioned with axis vertical near the base of a cylindrical water tank 1.98 m (6.5 ft.) diameter and 6.25 m (20.5 ft.) depth. Criticality is controlled and shutdown margin assured by three control rods in the form of aluminum or stainless-steel clad boron carbide or borated graphite. A fourth control rod would be used for 1,250-kW operation. A biological shield of reinforced concrete at least 2.5 m (8.2 ft) thick provides radiation shielding at the side and at the base the reactor tank. The tank and shield are in a 4078-m^3 (144,000 $ft.^3$) confinement building

Deleted: Original (12/04)

made of reinforced concrete and structural steel, with composite sheathing and aluminum siding. Sectional views of the reactor are shown in Figures 4.1 and 4.2.

Criticality was first achieved on October 16, 1962 at 8:25 p.m. In 1968 pulsing capability was added and the maximum steady-state operating power was increased from 100 kW to 250 kW. The original aluminum-clad fuel elements were replaced with stainless-steel clad elements in 1973. Coolant system was replaced (and upgraded in 2000), the reactor operating console was replaced, and the control room was enlarged and modernized in 1993, with support from the U.S. Department of Energy. All neutronic instrumentation was replaced in 1994.

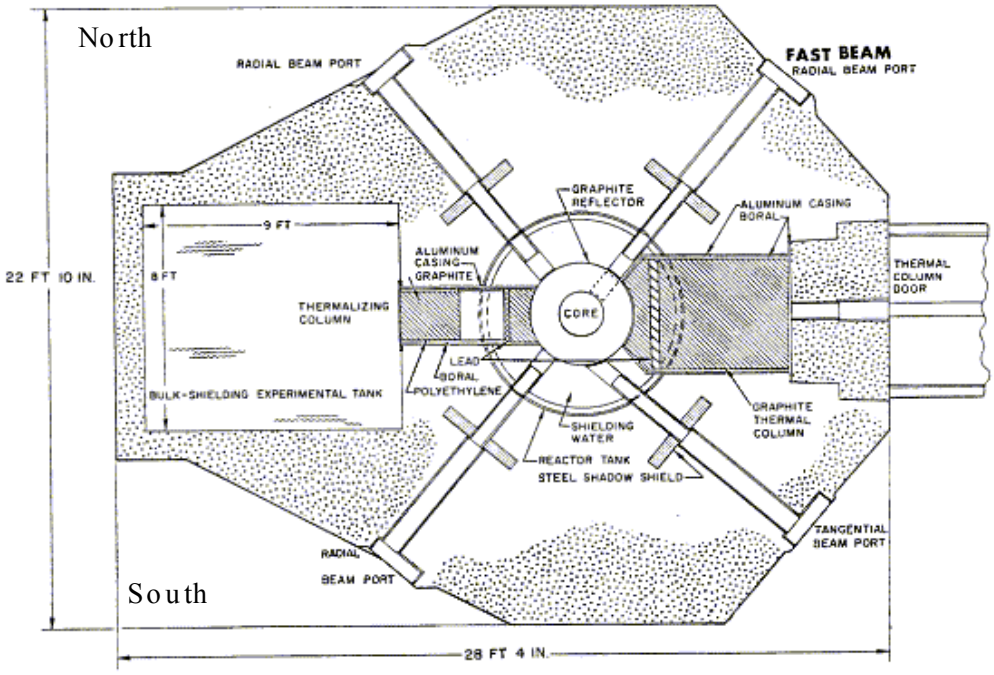

Figure 4. 1, Vertical Section Through the KSU TRIGA Reactor.

Deleted: Original (12/04)

4.2 Reactor Core

The General Atomics TRIGA reactor design began in 1956. The original design goal was a completely and inherently safe reactor. Complete safety means that all the available excess reactivity of the reactor can be instantaneously introduced without causing an accident. Inherent safety means that an increase in the temperature of the fuel immediately and automatically results in decreased reactivity through a prompt negative temperature coefficient. These features were accomplished by using enriched uranium fuel in a zirconium hydride matrix.

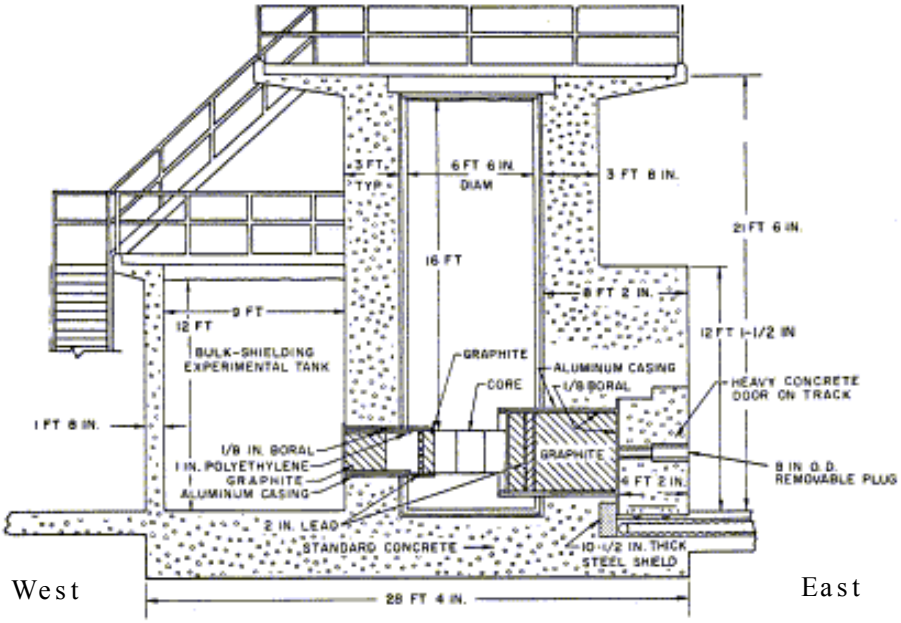

Figure 4. 2, Horizontal Section Through the KSU TRIGA Reactor.

The basic parameter providing the TRIGA system with a large safety factor in steady state and transient operations is a prompt negative temperature coefficient, relatively constant with temperature (-0.01% Δk/k°C). This coefficient is a function of the fuel composition and core geometry. As power and temperature increase, matrix changes cause a shift in the neutron energy spectrum in the fuel to higher energies. The uranium exhibits lower fission cross sections for the higher energy neutrons, thus countering the power increase. Therefore, fuel and clad temperature automatically limit operation of the reactor.

Deleted: Original (12/04)

It is more convenient to set a power level limit that is based on temperature. The design bases analysis indicates that operation at up to 1900 kW (with an 83 element core and 120°F inlet water temperature) with natural convective flow will not allow film boiling, and therefore high fuel and clad temperatures which could cause loss of clad integrity could not occur. An 85-element core distributes the power over a larger volume of heat generating elements, and therefore results in a more favorable, more conservative, thermal hydraulic response.

4.2.1 Reactor Fuel[1]

TRIGA fuel was developed around the concept of inherent safety. A core composition was sought which had a large prompt negative temperature coefficient of reactivity such that if all the available excess reactivity were suddenly inserted into the core, the resulting fuel temperature would automatically cause the power excursion to terminate before any core damage resulted. Zirconium hydride was found to possess a basic mechanism to produce the desired characteristic. Additional advantages were that ZrH has a high heat capacity, results in relatively small core sizes and high flux values due to the high hydrogen content, and could be used effectively in a rugged fuel element size.

TRIGA fuel is designed to assure that fuel and cladding can withstand all credible environmental and radiation conditions during its lifetime at the reactor site. As described in 3.5.1 (Fuel System) and NUREG 1282, fuel temperature limits both steady-state and pulse-mode operation. The fuel temperature limit stems from potential hydrogen outgassing from the fuel and the subsequent stress produced in the fuel element clad material. The maximum temperature limits of 1150°C (with clad < 500°C) and 950°C (with clad > 500°C) for U-ZrH ($H/Zr_{1.65}$) have been set to limit internal fuel cladding stresses that might challenge clad integrity (NUREG 1282). These limits are the principal design bases for the safety analysis.

a. Dimensions and Physical Properties.

The KSU TRIGA reactor is fueled by stainless steel clad Mark III fuel-elements. Three instrumented aluminum-clad Mark II elements are still available for use in the core. General properties of TRIGA fuel are listed in Table 4.1. The Mark III elements are illustrated in Figure 4.3. To facilitate hydriding in the Mk III elements, a zirconium rod is inserted through a 0.635 cm. (1/4-in.) hole drilled through the center of the active fuel section.

Instrumented elements have three chromel-alumel thermocouples embedded to about 0.762 cm (0.3 in.) from the centerline of the fuel, one at the axial center plane, and one each at 2.54 cm. (1 in.) above and below the center plane. Thermocouple leadout wires pass through a seal in the upper end fixture, and a leadout tube provides a watertight conduit carrying the leadout wires above the water surface in the reactor tank.

[1]Unless otherwise indicated, fuel properties are taken from the General Atomics report of Simnad [1980] and from authorities cited by Simnad.

Deleted: Original (12/04)

Graphite dummy elements may be used to fill grid positions in the core. The dummy elements are of the same general dimensions and construction as the fuel-moderator elements. They are clad in aluminum and have a graphite length of 55.88 cm (22 in.).

Table 4.1, Nominal Properties of Mark II and Mark III TRIGA Fuel Elements in use at the KSU Nuclear Reactor Facility.

Property	Mark II	Mark III
Dimensions		
Outside diameter, $D_o = 2r_o$	1.47 in. (3.7338 cm)	1.47 in. (3.7338 cm)
Inside diameter, $D_i = 2r_i$	1.41 in (3.6322 cm)	1.43 in. (3.6322 cm)
Overall length	28.4 in. (72.136 cm)	28.4 in. (72.136 cm)
Length of fuel zone, L	14 in. (35.56 cm)	15 in. (38.10 cm)
Length of graphite axial reflectors	4 in. (10.16 cm)	3.44 in (8.738 cm)
End fixtures and cladding	aluminum	304 stainless steel
Cladding thickness	0.030 in. (0.0762 cm)	0.020 in. (0.0508 cm)
Burnable poisons	Sm wafers	None
Uranium content		
Weight percent U	8.0	8.5
^{235}U enrichment percent	20	20
^{235}U content	36 g	38 g
Physical properties of fuel excluding cladding		
H/Zr atomic ratio	1.0	1.6
Thermal conductivity (W cm^{-1} K^{-1})	0.18	0.18
Heat capacity [T ≥0°C] (J cm^{-3} K^{-1})		2.04 + 0.00417T
Mechanical properties of delta phase U-ZrH[a]		
Elastic modulus at 20°C		9.1×10^6 psi
Elastic modulus at 650°C		6.0×10^6 psi
Ultimate tensile strength (to 650°C)		24,000 psi
Compressive strength (20°C)		60,000 psi
Compressive yield (20°C)		35,000 psi

[a]Source: Texas SAR [1991].

b. Composition and Phase Properties

The Mark III TRIGA fuel element in use at Kansas State University contains nominally 8.5% by weight of uranium, enriched to 20% ^{235}U, as a fine metallic dispersion in a zirconium hydride matrix. The H/Zr ratio is nominally 1.6 (in the face-centered cubic delta phase). The equilibrium hydrogen dissociation pressure is governed by the composition and temperature. For $ZrH_{1.6}$, the equilibrium hydrogen pressure is one atmosphere at about 760°C. The single-phase, high-hydride composition eliminates the problems of density changes associated with phase changes and with thermal diffusion of the hydrogen. Over 25,000 pulses have been performed with the TRIGA fuel elements at General Atomic, with fuel temperatures reaching peaks of about 1150°C.

Deleted: Original (12/04)

The zirconium-hydrogen system, whose phase diagram is illustrated in Chapter 3, is essentially a simple eutectoid, with at least four separate hydride phases. The delta and epsilon phases are respectively face-centered cubic and face-centered tetragonal hydride phases. The two phase delta + epsilon region exists between $ZrH_{1.64}$ and $ZrH_{1.74}$ at room temperature, and closes at $ZrH_{1.7}$ at 455°C. From 455°C to about 1050°C, the delta phase is supported by a broadening range of H/Zr ratios.

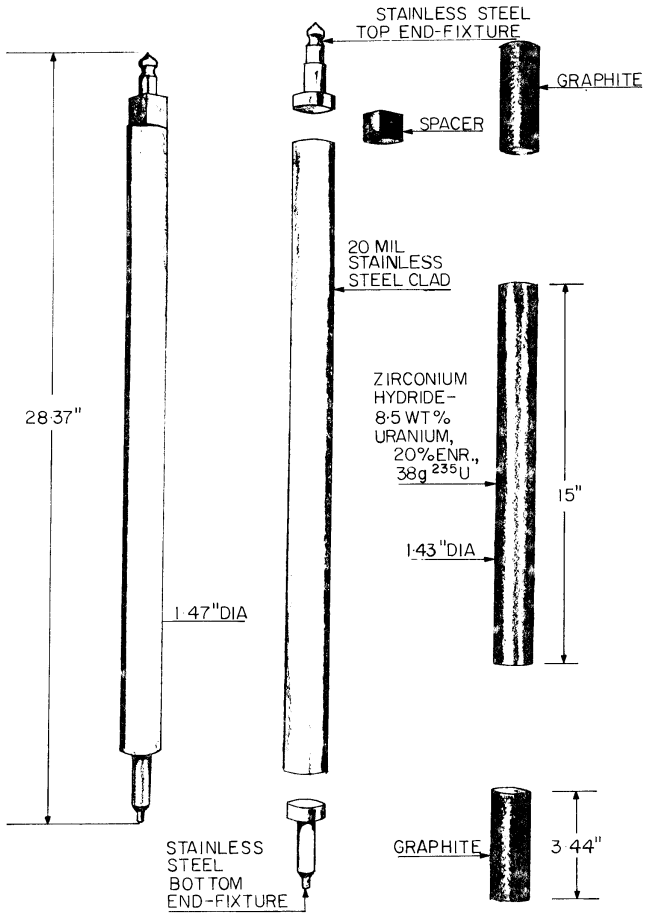

Figure 4.3, TRIGA Fuel Element.

Deleted: Original (12/04)

c. Core Layout

A typical layout for a KSU TRIGA II 250-kW core (Core II-18) is illustrated in Figure 4.4. The layout for the 1,250-kW core is expected to be similar, except that the graphite elements will be replaced by fuel elements, one additional control rod will be added, and control rod positions will be adjusted..

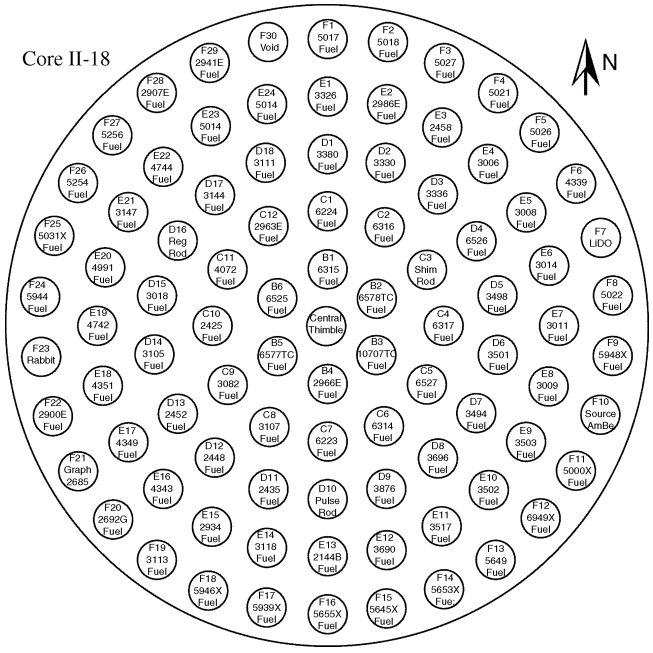

Figure 4.4, Core Layout (250 kW).

The additional fuel elements are required to compensate for higher operating temperatures from the higher maximum steady state power level. The additional control rod is required to meet reactivity control requirements at higher core reactivity associated with the additional fuel. The control rod positions will be different to allow a higher worth pulse rod (the 250 kW pulse rod reactivity worth is $2.00, the 1,250 kW core pulse rod reactivity worth is $3.00), balancing the remaining control rod's worth to meet minimum shutdown margin requirements, and meeting physical constraints imposed by the dimensions of the pool bridge

Deleted: Original (12/04)

4.2.2 Control Rods

The pulse rod is 3.175 cm. (1.25 in.) diameter. Other rods are 2.225 cm (7/8 in.) diameter. Control rods are 50.8 cm. (20 in.) long boron carbide or borated graphite, clad with a 0.0762 cm. (30-mil) aluminum sheath.

The control rod drives are connected to the control rod clutches through three extension shafts. The clutch and upper extension shaft for standard rods extend through an assembly designed with slots that provides a hydraulic cushion (or buffer) for the rod during a scram, and also limits the bottom position of the control rods so that they do not impact the bottom of the control rod guide tube (in the core). The buffers for two standard rods are shown in the left hand picture below (slotted tubes on the right hand side) along with the top section of the pulse/transient rod extension. The pulse rod drive clutch connects to a solid extension shaft through a pneumatic cylinder; the dimensions of the cylinder limits bottom travel.

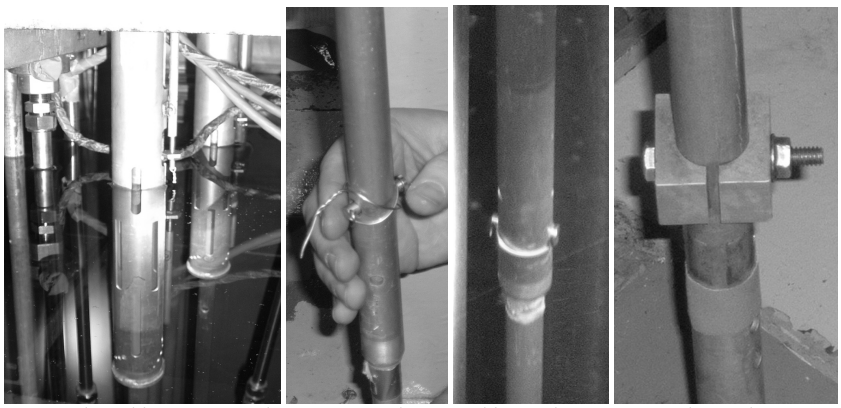

Upper Pulse, Shim & Reg Rods Reg Rod Shim Rod Pulse Rod

Figure 4.5, Control Rod Upper Extension Assemblies

The bottom of the pulse rod is shown on the left hand side of Figure 4.5. The upper extension shaft is a hollow tube, the middle extension is solid. The upper extension shaft is connected to the middle extension shaft with lock wire or a pin and lock wire for standard rods, with a bolted collar for the pulse rod (the mechanical shock during a pulse requires a more sturdy fastener). Securing the upper control rod extension to the middle extension at one of several holes drilled in the upper part of the middle extension (Figure 4.6) provides adjustment for the control rods necessary to ensure the control rod full in position is above the bottom of the guide tube.

Deleted: Original (12/04)

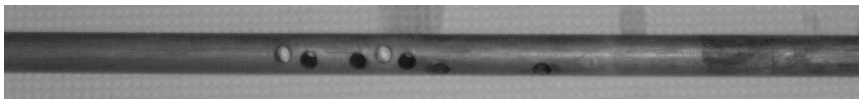

Figure 4.6, Middle Extension Rod Alignment Holes

The middle solid extension is similarly connected to the lower extension. The lower extension is hollow, the middle extension fits into the lower extension and a hole drilled in the overlap secures the lower extension to the middle extension. Typically the lower extension has a tighter fit than the upper extension because the lower and middle extension are not separated for inspections and because the interface with upper extension is used to set the bottom position of the control rod. Pictures of the lower connector for the pulse rod and one standard rod are shown at the left in Figure 4.7..

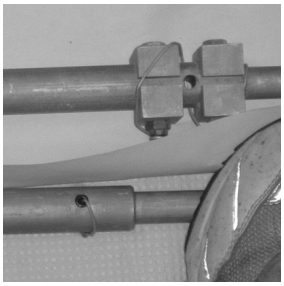

Figure 4.7, Standard & Pulse Rod Lower Coupling

The bottom of the lower extension attaches directly to the control rod. Pictures of the control rods taken during the 2003 control rod inspection are in Figure 4.8. The rods move within control rod guide tubes, shown in Figure 4.9. The guide tubes have perforated walls. The guide tubes have a small metal wire in the tip that fits into the lower grid plate; a setscrew inside the bottom of the guide tube pushes the wire against the lower grid plate to secure the guide tube.

Deleted: Original (12/04)

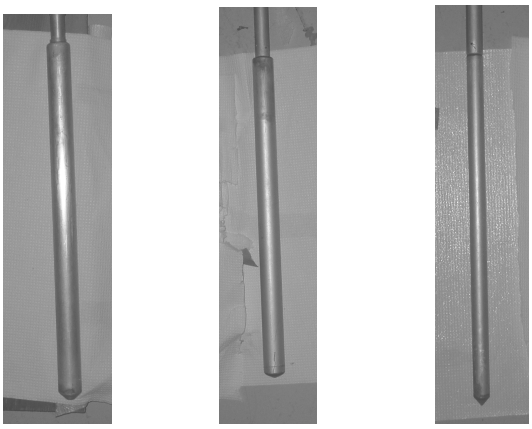

Pulse Rod Shim Rod Reg Rod

Figure 4.8, Control Rods During 2003 Inspection

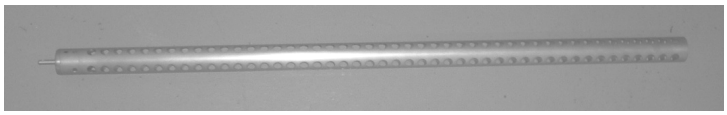

Full Guide Tube

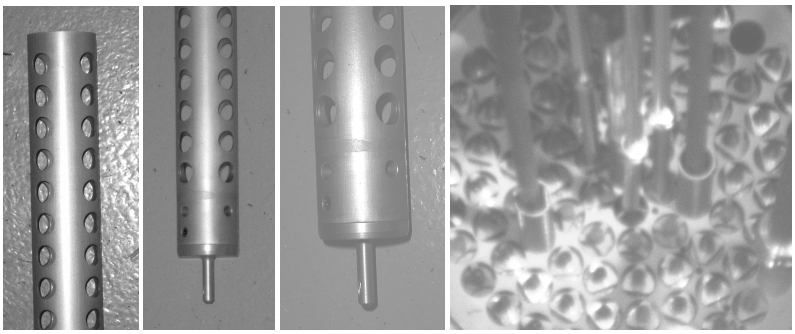

Upper Lower Lower Detail Position in Upper Grid Plate

Figure 4.9, Control Rod Guide Tubes

Deleted: Original (12/04)

a. Control Function

While three control rods were adequate to meet Technical Specification requirements for reactivity control with the 100 kW and 250 kW cores, reactivity limits for operation at a maximum power level of 1,250 kW requires four control rods (three standard and one transient/pulsing control rod). Although four control rods are required to operate at the maximum power level of 1,250 kW, all Technical Specification requirements are met with a minimum of three operable control rods, provided that the inoperable control rod is fully inserted. Inoperable control rods that are fully inserted do not negatively impact the minimum safety shutdown margin or maximum core excess reactivity. Furthermore, the reduction in maximum achievable power level associated with the inoperable control rod fully inserted results in a maximum temperature in any fuel element that is less than the highest temperature in a fuel element in the B-ring with all control rods fully withdrawn.

The control-rod drives are mounted on a bridge at the top of the reactor tank. The control rod drives are coupled to the control rod through a connecting rod assembly that includes a clutch. The standard rod clutch is an electromagnet; the transient rod clutch is an air-operated shuttle. Scrams cause the clutch to release by de-energizing the magnetic clutch and venting air from the transient rod clutch; gravity causes the rod to fall back into the core. Interlocks ensure operation of the control rods remains within analyzed conditions for reactivity control, while scrams operation at limiting safety system settings. A detailed description of the control-rod system is provided in Chapter 7; a summary of interlocks and scrams is provided below in Table 4.2 and 4.3. Note that (1) the high fuel temperature and period scrams are not required, (2) the fuel temperature scram limiting setpoint depends on core location for the sensor, and (3) the period scram can be prevented by an installed bypass switch.

Table 4.2, Summary of Control Rod Interlocks

INTERLOCK	SETPOINT	FUNCTION/PURPOSE
Source Interlock	2 cps	Inhibit standard rod motion if nuclear instrument startup channel reading is less than instrument sensitivity/ensure nuclear instrument startup channel is operating
Pulse Rod Interlock	Pulse rod inserted	Prevent applying power to pulse rod unless rod inserted/prevent inadvertent pulse
Multiple Rod Withdrawal	Withdraw signal, more than 1 rod	Prevent withdrawal of more than 1 rod/Limit maximum reactivity addition rate
Pulse Mode Interlock	Mode switch in Hi Pulse	Prevent withdrawing standard control rods in pulse mode
Pulse-Power Interlock	10 kW	Prevent pulsing if power level is greater than 10 kW

NOTE: (1) Pulse-Power Interlock normally set at 1 kW, (2) only Pulse Mode Interlock required by Technical Specifications

Formatted: Font:Not Bold

Formatted: Normal, Left, Indent: Left: 0"

Deleted: Original (12/04)

b. Evaluation of Control Rod System

The reactivity worth and speed of travel for the control rods are adequate to allow complete control of the reactor system during operation from a shutdown condition to full power. The TRIGA system does not rely on speed of control as significant for safety of the reactor; scram times for the rods are measured periodically to monitor potential degradation of the control rod system. The inherent shutdown mechanism (temperature feedback) of the TRIGA prevents unsafe excursions and the control system is used only for the planned shutdown of the reactor and to control the power level in steady state operation.

Table 4.3, Summary of Reactor SCRAMs

Measuring Channel	Limiting Trip Setpoint		Actual Setpoint
	Steady State	Pulse	
Linear Channel High Power	110%	N/A	104%
Power Channel High power	110%	N/A	104%
Detector High Voltage	90%	90%	90%
High Fuel Temperature[1]	600°C B Ring element		450°C
	555°C C Ring element		
	480°C D Ring element		
	380°C E Ring element		350°C
Period [1]	N/A	N/A	3 sec

NOTE [1]: Period trip and temperature trip are not required by Technical Specifications

The reactivity worth of the control system can be varied by the placement of the control rods in the core. The control system may be configured to provide for the excess reactivity needed for 1,250 kW operations for eight hours per day (including xenon override) and will assure a shutdown margin of at least $0.50.

Nominal speed of the standard control rods is about 12 in. (30.5 cm) per minute (with the stepper motor specifically adjusted to this value), of the transient rod is about 24 in. (61 cm) per minute, with a total travel about 15 in. (38.1 cm). Maximum rate of reactivity change for standard control rods is specified in Technical Specifications.

4.2.3 Neutron Moderator and Reflector

Hydrogen in the Zr-H fuel serves as a neutron moderator. Demineralized light water in the reactor pool also provides neutron moderation (serving also to remove heat from operation of the reactor and as a radiation shield). Water occupies approximately 35% of the core volume. A graphite

Deleted: Original (12/04)

reflector surrounds the core, except for a cutout containing the rotary specimen rack (described in Chapter 10). Each fuel element contains graphite plugs above and below fuel approximately 3.4 in. in length, acting as top and bottom reflectors.

The radial reflector is a ring-shaped, aluminum-clad, block of graphite surrounding the core radially. The reflector is 0.457-m (18.7 in.) inside diameter, 1.066-m (42 in.) outside diameter, and 0.559-m (20 in.) height. Embedded as a circular well in the reflector is an aluminum housing for a rotary specimen rack, with 40 evenly spaced tubular containers, 3.18-cm (1.25 in.) inside diameter and 27.4-cm (10.8 in.) height. The rotary specimen rack housing is a watertight assembly located in a re-entrant well in the reflector.

The radial reflector assembly rests on an aluminum platform at the bottom of the reactor tank. Four lugs are provided for lifting the assembly. A radial void about 6 inches (15.24 cm) in diameter is located in the reflector such that it aligns with the radial piercing beam port (NE beam port). The reflector supports the core grid plates, with grid plate positions set by alignment fixtures. Graphite inserts within the fuel cladding provide additional reflection. Inserts are placed at both ends of the fuel meat, providing top and bottom reflection.

4.2.4 Neutron Startup Source

A 2-curie americium-beryllium startup source (approximately 2×10^6 n s^{-1}) is used for reactor startup. The source material is encapsulated in stainless steel and is housed in an aluminum-cylinder source holder of approximately the same dimensions as a fuel element. The source holder may be positioned in any one of the fuel positions defined by the upper and lower grid plates. A stainless-steel wire may be threaded through the upper end fixture of the holder for use in relocating the source manually from the 22-ft level (bridge level) of the reactor.

4.2.5 Core Support Structure

The fuel elements are spaced and supported by two 0.75-in. (1.9 cm) thick aluminum grid plates. The grid plates have a total of 91 spaces, up to 85 of which are filled with fuel-moderator elements and dummy elements, and the remaining spaces with control rods, the central thimble, the pneumatic transfer tube, the neutron source holder, and one or more voids. The bottom grid plate, which supports the weight of the fuel elements, has holes for receiving the lower end fixtures. Space is provided for the passage of cooling water around the sides of the bottom grid plate and through 36 special holes in it. The 1.5-in. (3.8 cm) diameter holes in the upper grid plate serve to space the fuel elements and to allow withdrawal of the elements from the core. Triangular-shaped spacers on the upper end fixtures allow the cooling water to pass through the upper grid plate when the fuel elements are in position. The reflector assembly supports both grid plates.

4.3 Reactor Tank

The KSU TRIGA reactor core support structure rests on the base of a continuous, cylindrical aluminum tank surrounded by a reinforced, standard concrete structure (with a minimum

Deleted: Original (12/04)

thickness of approximately 249 cm. or 8 ft 2 in), as illustrated in Figures 4.1 and 4.2. The tank is a welded aluminum structure with 0.635 cm. (1/4-in.) thick walls. The tank is approximately 198 cm (6.5-ft) in diameter and approximately 625 cm (20.5-ft) in depth. The exterior of the tank was coated with bituminous material prior to pouring concrete to retard corrosion. Each experiment facility penetration in the tank wall (described below) has a water collection plenum at the penetration. All collection plenums are connected to a leak-off volume through individual lines with isolation valves, with the leak-off volumes monitored by a pressure gauge. The bulk shield tank wall is known to have a small leak into the concrete at the thermalizing column plenum, therefore a separate individual leak-off volume (and pressure gauge) is installed for the bulk shield tank; all other plenums drain to a common volume. In the event of a leak from the pool through an experiment facility, pressure in the volume will increase; isolating individual lines allows identification of the specific facility with the leak.

A bridge of steel plates mounted on two rails of structural steel provides support for control rod drives, central thimble, the rotary specimen rack, and instrumentation. The bridge is mounted directly over the core area, and spans the tank. Aluminum grating with clear plastic attached to the bottom is installed that can be lowered over the pool. The grating can be lowered when activities could cause objects or material to fall into the reactor pool. The grating normally remains up to reduce humidity at electro-mechanical components of the control rod drive system and to prevent the buildup of radioactive gasses at the pool surface during operations.

Four beam tubes run from the reactor wall to the outside of the concrete biological shield in the outward direction. Tubes welded to the inside of the wall run toward the reactor core. Three of the tubes (NW, SW, and SE) end at the radial reflector. The NE beam tube penetrates the radial reflector, extending to the outside of the core. Two penetrations in the tank allow neutron extraction into a thermal column and a thermalizing column (described in Chapter 10).

4.4 Biological Shield

The reactor tank is surrounded on all sides by a monolithic reinforced concrete biological shield. The shielding configuration is similar to those at other TRIGA facilities operating at power levels up to 1 MW. Above ground level, the thickness varies from approximately 249 cm. (8 ft 2 in.) at core level to approximately 91 cm. (3 ft.) at the top of the tank.

The massive concrete bulk shield structure provides additional radiation shielding for personnel working in and around the reactor laboratory and provides protection to the reactor core from potentially damaging natural phenomena.

4.5 Nuclear Design

The strong negative temperature coefficient is the principal method for controlling the maximum power (and consequently the maximum fuel temperature) for TRIGA reactors. This coefficient is a function of the fuel composition, core geometry, and temperature. For fuels with 8.5% U, 20% enrichment, the value is nearly constant at 0.01% Δk/k per °C, and varies only weakly dependent on geometry and temperature.

Deleted: Original (12/04)

Fuel and clad temperature define the safety limit. A power level limit is calculated that ensures that the fuel and clad temperature limits will not be exceeded. The design bases analysis indicates that operation at 1,250 kW thermal power with an 83-element across a broad range of core and coolant inlet temperatures with natural convective flow will not allow film boiling that could lead to high fuel and clad temperatures that could cause loss of clad integrity.

Increase in maximum thermal power from 250 to 1,250 kW does not affect fundamental aspects of TRIGA fuel and core design, including reactivity feedback coefficients, temperature safety limits, and fission-product release rates. Thermal hydraulic performance is addressed in Section 4.6.

4.5.1 Design Criteria - Reference Core

The limiting core configuration for this analysis is a compact core defined by the TRIGA Mk II grid plates (Section 4.2.5). The grid plates have a total of 91 spaces, up to 85 of which are filled with fuel-moderator elements and graphite dummy elements, and the remaining spaces with control rods, the central thimble, the pneumatic transfer tube, the neutron source holder, and one or more voids in the E or F (outermost two rings) as required to support experiment operations or limit excess reactivity. The bottom grid plate, which supports the weight of the fuel elements, has holes for receiving the lower end fixtures.

4.5.2 Reactor Core Physics Parameters

The limiting core configuration differs from the configuration prior to upgrade only in the addition of a fourth control rod, taking the place of a graphite dummy element or void experimental position. For this reason, core physics is not affected by the upgrade except for linear scaling with power of neutron fluxes and gamma-ray dose rates.

For comparison purposes, a tabulation of total rod worth for each control element from the K-State reactor from a recent rod worth measurement is provided with the values from the Cornell University TRIGA reactor as listed in NUREG 0984 (Safety Evaluation Report Related to the Renewal of the Operating license for the Cornell University TRIGA Research Reactor).

Table 4.4, 250 kW Core Parameters.

β (effective delayed neutron fraction)	0.007
ℓ (effective neutron lifetime)	43 μs
α_{Tf} (prompt temperature coefficient)	-\$0.017 °C^{-1} @ 250kW ~275 °C
α_V (void coefficient)	-0.003 1%$^{-1}$ void
α_p (power temperature coefficient – weighted ave)	-\$0.006 kW^{-1} to – \$0.01 kW^{-1}

Deleted: :S

Deleted: E

Deleted: E

Deleted: Original (12/04)

Table 4.5, Comparison of Control Rod Worths.

	KSU TRIGA Mark II (250 kW) Core II-19		Core III-1		Cornell University (500 kW)	
Pulse	D-10	$1.96	C-4	$2.12	D-10	$1.88
Shim	C-3	$2.88	D-4	$1.85	D-16	$2.20
Safety	NA	$0.0	D-16	$1.82	D-4	$1.99
Regulating	D-16	$1.58	E-1	$0.79	E-1	$0.58
TOTAL	NA	$6.42	NA	$6.58	NA	$6.65

NOTE: Core III-1 has an experiment positioned to control the worth of the pulse rod
The pulse rod is similar to a standard control rod, and the worth of the pulse rod compares well with the comparable standard control rods in similar ring positions. A maximum pulse is analyzed for thermal hydraulic response and maximum fuel temperature.

4.5.3 Fuel and Clad Temperatures

This section analyzes expected fuel and cladding temperatures with realistic modeling of the fuel-cladding gap. Analysis of steady state conditions reveals maximum heat fluxes well below the critical heat flux associated with departure from nucleate boiling. Analysis of pulsed-mode behavior reveals that film boiling is not expected, even during or after pulsing leading to maximum adiabatic fuel temperatures.

Chapter 4, Appendix A of this chapter reproduces a commonly cited analysis of TRIGA fuel and cladding temperatures associated with pulsing operations. The analysis addresses the case of a fuel element at an average temperature of 1000°C immediately following a pulse and estimates the cladding temperature and surface heat flux as a function of time after the pulse. The analysis predicts that, if there is no gap resistance between cladding and fuel, film boiling can occur very shortly after a pulse, with cladding temperature reaching 470°C, but with stresses to the cladding well below the ultimate tensile strength of the stainless steel. However, through comparisons with experimental results, the analysis concludes that an effective gap resistance of 450 Btu hr^{-1} ft^{-2} $°F^{-1}$ (2550 W m^{-2} K^{-1}) is representative of standard TRIGA fuel and, with that gap resistance, film boiling is not expected. This section provides an independent assessment of the expected fuel and cladding thermal conditions associated with both steady-state and pulse-mode operations.

a. Spatial Power Distribution

The following conservative approximations are made in characterizing the spatial distribution of the power during steady-state operations.

- The hottest fuel element delivers twice the power of the average.

  Classically, the radial hot-channel factor for a cylindrical reactor (using R as the physical radius and R_e as the physical radius and the extrapolation distance) is given[2] by:

[2] Elements of Nuclear Reactor Design, 2nd Edition (1983), J. Weisman, Section 6.3

Deleted: Original (12/04)

$$F^{N}_{R_0} = \frac{1.202 * \left(R / R_e \right)}{J_1 \left[2.4048 * \left(R / R_e \right) \right]}$$

with a radial peaking factor of 1.93 for the KSU TRIGA II geometry,. However, TRIGA fuel elements are on the order of a mean free path of thermal neutrons, and there is a significant change in thermal neutron flux across a fuel element. Calculated thermal neutron flux data[3] indicates that the ratio of peak to average neutron flux (peaking factor) for TRIGA cores under a range of conditions (temperature, fuel type, water and graphite reflection) has a small range of 1.36 to 1.40.

Actual power produced in the most limiting actual case is 14% less than power calculated using the assumption; therefore using a peaking factor of 2.0 to determine calculated temperatures and will bound actual temperatures by a large margin, and is extremely conservative.

- The axial distribution of power in the hottest fuel element is sinusoidal, with the peak power a factor of $\pi/2$ times the average, and heat conduction radial only.

  The axial factor for power produced within a fuel element is given by:

$$g(z) = 1.514 * \cos\left(\frac{\pi}{2} * \frac{z}{2 * \ell + \ell_{ext}} \right) \quad (1)$$

  in which $\ell = L/2$ and ℓ_{ext} is the extrapolation length in graphite, namely, 0.0275 m. The value used to calculate power in the limiting location within the fuel element is therefore 4% higher a power calculated with the actual peaking factor. Actual power produced in the most limiting actual case is 4% less than power calculated using the assumption; therefore calculated temperatures will bound actual temperatures.

- The location on the fuel rod producing the most thermal power with thermal power distributed over 83 fuel rods is therefore:

$$q''_{max} = \frac{P}{83 \cdot \pi \cdot D_0 \cdot L} \cdot \frac{\pi}{2} \cdot 2 = \frac{P}{83 \cdot D_0 \cdot L} = P \cdot 0.8469 \quad (2)$$

- The radial and axial distribution of the power within a fuel element is given by

[3] GA-4361, Calculated Fluxes and Cross Sections for TRIGA Reactors (8/14/1963), G. B. West

Formatted: Not Raised by / Lowered by
Formatted: Equation, Left
Deleted: → → →
Deleted: 6
Field Code Changed
Field Code Changed
Formatted: Not Raised by / Lowered by
Deleted: → → →
Deleted: 7
Formatted: Equation, Indent: Left: 0.5", Hanging: 0.5"
Deleted: Original (12/04)

$$q'''(r,z) = q'''_{avg} f(r) g(z), \quad (3)$$

in which r is measured from the vertical axis of the fuel element and z is measured along the axis, from the center of the fuel element. The axial peaking factor follows from the previous assumption of the core axial peaking factor, but (since there is a significant flux depression across a TRIGA fuel element) distribution of power produced across the radius of the fuel the radial peaking factor requires a different approach than the previous radial peaking factor for the core.

- The radial factor is given by:

$$f(r) = \frac{a + cr + er^2}{1 + br + dr^2}, \quad (4)$$

in which the parameters of the rational polynomial approximation are derived from flux-depression calculations for the TRIGA fuel (Ahrens 1999a). Values are: a = 0.82446, b = -0.26315, c = -0.21869, d = -0.01726, and e = +0.04679. The fit is illustrated in Figure 4.11.

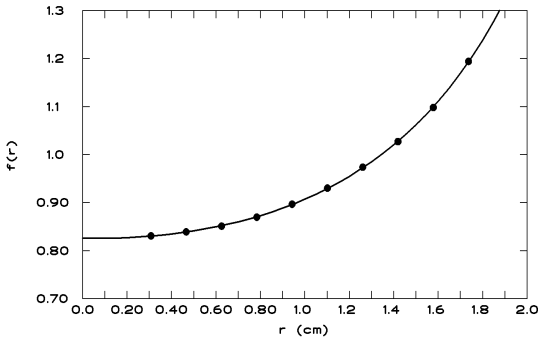

Figure 4.12, Radial Variation of Power Within a TRGIA Fuel Rod.
(Data Points from Monte Carlo Calculations [Ahrens 1999a])

b. Heat Transfer Models

The overall heat transfer coefficient relating heat flux at the surface of the cladding to the difference between the maximum fuel (centerline) temperature and the coolant temperature can be calculated as the sum of the temperature changes through each element from the centerline of the fuel rod to the water coolant, where the subscripts for each of the ΔT's represent changes between bulk water temperature and cladding outer surface, (br_0), changes between cladding outer surface and cladding inner surface (r_0r_i), cladding inner surface and fuel outer surface – gap (g), and the fuel outer surface to centerline (r_icl):

Deleted: 5
Deleted: 7
Deleted: a
Formatted: Normal, Left
Deleted:
Deleted: Original (12/04)

$$T_{cl} = T_b + \Delta T_{br_0} + \Delta T_{r_0 r_i} + \Delta T_g + \Delta T_{r_i cl} \quad (5)$$

A standard heat resistance model for this system is:

$$T_{cl} = T_b + q'' \left[\frac{1}{h} + \frac{r_0 \ln\left(r_o / r_i\right)}{k_c} + \frac{r_0}{r_i h_g} + \frac{r_0}{2k_f} \right] \quad (6)$$

and heat flux is calculated directly as:

$$q'' = U\Delta T = \frac{T_{\max} - T_b}{\frac{1}{h} + \frac{r_o \ln(r_o / r_i)}{k_c} + \frac{r_o}{r_i h_g} + \frac{r_o}{2k_f}}, \quad (7)$$

in which r_o and r_i are cladding inner and outer radii, h_g is the gap conductivity, h is the convective heat transfer coefficient, and k_f is the fuel thermal conductivity. The gap conductivity of 2840 W m^{-2} K^{-1} (500 Btu h^{-1} ft $^{-2}$ $°F^{-1}$) is taken from Appendix A. The convective heat transfer coefficient is mode dependent and is determined in context. Parameters are cross-referenced to source in Table 4.6.

Table 4.6: Thermodynamic Values

Parameter	Symbol	Value	Units	Reference
Fuel conductivity	k_f	18	W m^{-1} K^{-1}	Table 13.3
Clad conductivity	k_g	14.9	W m^{-1} K^{-1} (300 K)	Table 13.3
		16.6	W m^{-1} K^{-1} (400 K)	Table 13.3
		19.8	W m^{-1} K^{-1} (600 K)	Table 13.3
Gap resistance	h_g	2840	W m^{-2} K^{-1}	Appendix A
Clad outer radius	r_0	0.018161	M	Table 13.1
Fuel outer radius	r_i	0.018669	M	Table 13.1
Active fuel length	L_f	0.381	M	Table 13.1
No. fuel elements	N	83	N/A	Chap 13
Axial peaking factor	APF	$\pi/2$	N/A	Table 13.4

General Atomics reports that fuel conductivity over the range of interest has little temperature dependence, so that:

$$\frac{r_0}{2k_f} = 5.1858\text{E-}04 \frac{\text{m}^2 K}{\text{W}}$$

Gap resistance has been experimentally determined as indicated, so that:

Deleted: Eq. 1

Deleted: Eq. 2

Deleted: 2

Deleted: Original (12/04)

$$\frac{r_0}{r h_g} = 3.6196\text{E-}04 \frac{\text{m}^2 K}{\text{W}}$$

Temperature change across the cladding is temperature dependent, with values quoted at 300 K, 400 K and 600 K. Under expected conditions, the value for 127°C applies so that:

$$\frac{r_0 \ln \frac{r_0}{r_i}}{k_c} = 3.103e-5 \frac{m^2 K}{W}$$

Table 4.7, Cladding Heat Transfer Coefficient

Temp (°K)	Temp (°C)	m^2 K W^{-1}
300	27	3.457e-5
400	127	3.103e-5
600	327	2.601e-5

Deleted: w

It should be noted that, since these values are less than 10% of the resistance to heat flow attributed to the other components, any errors attributed to calculating this factor are small.

The convection heat transfer coefficient was calculated at various steady state power levels. A graph of the calculated values results in a nearly linear response function.

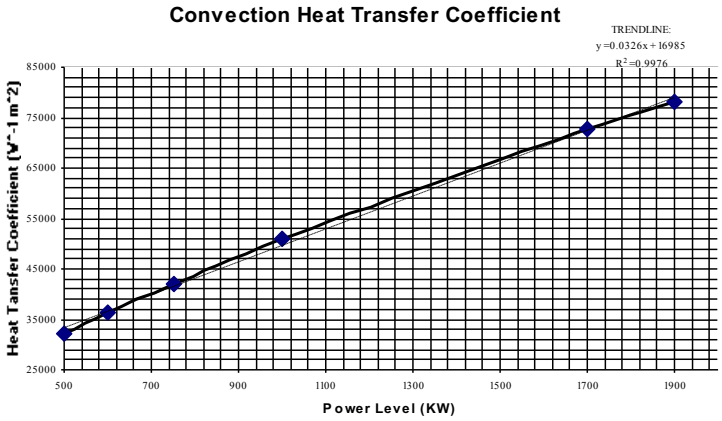

Figure 4.10, Convection Hear Transfer Coefficient versus Power Level

Deleted: Original (12/04)

$$\frac{1}{h} = \frac{1}{0.0326P(watts) + 16985}$$

Core centerline temperature for the fuel rod producing the maximum heat as a function of power can be calculated as:

$$T_{cl} = T_b + 0.423P\left[\frac{1}{0.0326P + 16985} + 3.103e-5 + 3.620e-4 + 5.186e-4\right] \quad (8)$$

Deleted: 10

c. Steady-State Mode of Operation

Centerline temperature calculations were performed on a "reference core" using the model as described above for the hottest location in the core. The reference core contains 83 fuel elements; temperature calculations using the reference core are conservative because at least 83 elements are required for steady state 500 kW operations, while analysis assumes 1.25 MW operation. A core with more than 83 elements will distribute heat production across a larger number of fuel elements, resulting in a lower heat flux per fuel rod than calculations based on the reference core. Since actual heat production will be less than heat calculated in analysis, actual temperatures will be lower. A power level of 1.25 MW steady state power at 20°C and 100°C was assumed with the following results:

Deleted: T

Deleted: were made

Table 4.8, Calculated Temperature Data for 1,250 kW Operation

Fuel Centerline °C	Fuel/Gap Interface °C	Gap/Clad Interface °C	Clad/Water Interface °C	Bulk Water °C
503.2	229.0	37.7	21.2	20.0
582.0	307.8	116.4	100.0	100.0

For the purposes of calculation, the two extremes of cladding thermal conductivity were assumed (300 K value and 600 K value) to determine expected centerline temperature as a function of power level. Calculations show the effects of thermal conductivity changes are minimal. The graph also shows that fuel temperature remains below about 750 °C at power levels up to 1900 kW with pool temperature at 27 °C (300 K), and 1700 kW with pool temperatures at 100 °C.

Deleted: Original (12/04)

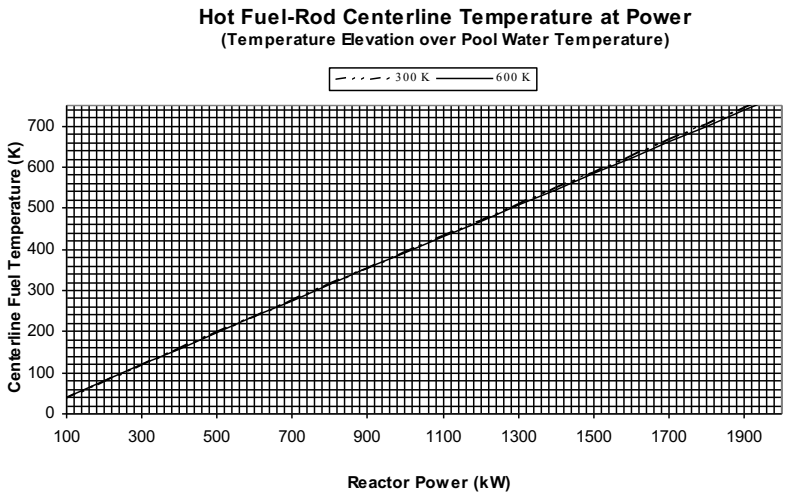

Figure 4.11, Hot Fuel-Rod Centerline Temperature

For the analysis of critical heat flux, a single channel model was built in RELAP-5/MOD 3.3 patch 04 (Feldman 2008). A snapshot of the model is presented in Figure 4.12. It has two time-dependent volumes, enforcing the pressure boundary conditions, and two pipes, simulating the cold and hot channel connected via a single junction component of RELAP. Heat is added to the fluid by incorporating the heat structure component (simulating a fuel element) of RELAP with an appropriate axial power profile and power level. In this analysis, the power level for the B ring is at 24 kW (corresponding to an 85-element core with a ring-to-average peaking factor of 1.63). This power level is applied to the heat structure within the single channel. The model assumes an operating pressure of 143 kPa, and an operating temperature of 322.15 K (49.15°C).

The version of the RELAP code licensed to KSU uses PG-CHF correlation which is a state of the art best estimate CHF correlation developed by Nuclear Research institute of Rez in the Czech Republic. It is based on data in the Czech Republic data bank from 173 different sets of tube data, 23 sets of annular data, and 153 sets of rod bundle data. There are four forms of the PG-CHF correlation `Basic', `Flux', `Geometry', and `Power'. For the rod bundle it is applicable in the pressure range of 0.28 MPa to 18.73 MPa, for a mass flux of 34.1 to 7478 kg/s-m2, for 0.4-7.0 m length and for a diameter of 0.00241 to 0.07813 m. TRIGA has an operating pressure of 0.143 MPa and fuel rod length of 0.381 m, thus the operating conditions fall outside the range of the applicability of the PG-CHF correlation, and a different correlation is required to assess the departure from nucleate boiling ratio (DNBR ratio). One such correlation which is applicable for the low pressure range observed in TRIGA reactor facility is the Bernath correlation (Bernath 1960). The functional form of the Bernath correlation can be presented in the following equations.

Formatted ... [2]
Formatted ... [3]
Formatted ... [4]
Formatted ... [5]
Formatted ... [6]
Formatted ... [7]
Formatted ... [8]
Formatted ... [9]
Formatted ... [10]
Formatted ... [11]
Formatted ... [12]
Formatted ... [13]
Formatted ... [14]
Formatted ... [15]
Formatted ... [16]
Formatted ... [17]
Formatted ... [18]
Formatted ... [19]
Formatted ... [20]
Formatted ... [21]
Formatted ... [22]
Formatted ... [23]
Formatted ... [24]
Formatted ... [25]
Formatted ... [26]
Formatted ... [27]
Formatted ... [28]
Formatted ... [29]
Formatted ... [30]
Formatted ... [31]
Formatted ... [32]
Formatted ... [33]
Formatted ... [34]
Formatted ... [35]
Formatted ... [36]
Formatted ... [37]
Formatted ... [38]
Formatted ... [39]
Formatted ... [40]
Formatted ... [41]
Deleted: Original (12/04)

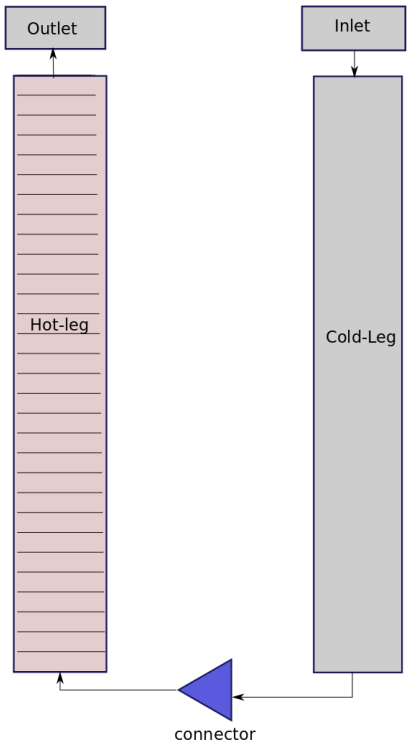

Figure 4.12 - RELAP single channel model used in CHF analysis

$$Q''_{BO} = h_{BO}\left(T_{wBO} - T_b\right) \quad (9)$$

$$h_{BO} = 10890\left(\frac{D_h}{D_h + D_H}\right) + \Delta v \quad (10)$$

Formatted: Centered, Keep with next

Formatted: Caption, Centered

Formatted: Don't adjust space between Latin and Asian text, Don't adjust space between Asian text and numbers, Tabs: 3", Centered + 6", Right

Deleted: 8

Formatted: Justified, Don't adjust space between Latin and Asian text, Don't adjust space between Asian text and numbers, Tabs: 3", Centered + 6", Right

Deleted:

Deleted: 8

Deleted: Original (12/04)

$$\Delta = \frac{48}{D_h^{0.6}}, \text{if } D_h \le 0.1 ft$$

$$\Delta = \frac{10}{D_h} + 90, \text{if } D_h \ge 0.1 ft$$

h_{BO} = film coefficient at CHF

D_h = hydraulic diameter (ft)

v = coolant velocity (ft / s)

T_{wBO} = wall temperature at burnout (°C)

D_H = heated diameter (ft)

The RELAP simulations were performed for the hot channel, i.e., a channel with a radial peaking factor of 1.63, assuming an 85-element core load and a power of 1.25 MWth, in order to obtain the pressure, temperature, and velocity distribution at different axial locations. With these calculations and the functional form of the Bernath correlation, the axial distribution of CHF was estimated in the hot channel. The methodology adopted for this analysis is described in literature (Feldman 2008). The hot channel model was based on the smallest hydraulic diameter in the core (between the A-ring and two B-ring elements) and the highest radial peaking factor. In the KSU TRIGA, the A-ring is occupied by the central thimble, not a fuel element. Since the actual hot channel would be between two B-ring elements and a C-ring element, the real hydraulic diameter will be slightly larger and the real heat flux into the channel will be slightly lower than the values assumed in the model. Therefore, this model is conservative in this regard.

The axial CHF results from the PG and Bernath heat flux models are shown in Figure 4.13 and Figure 4.14. The DNBR ratio exceeds 2.0 for all locations along the heated length of the hot channel.

Formatted: Centered, Don't adjust space between Latin and Asian text, Don't adjust space between Asian text and numbers, Tabs: 3", Centered + 5.5", Right

Formatted: Justified, Don't adjust space between Latin and Asian text, Don't adjust space between Asian text and numbers

Deleted: Original (12/04)

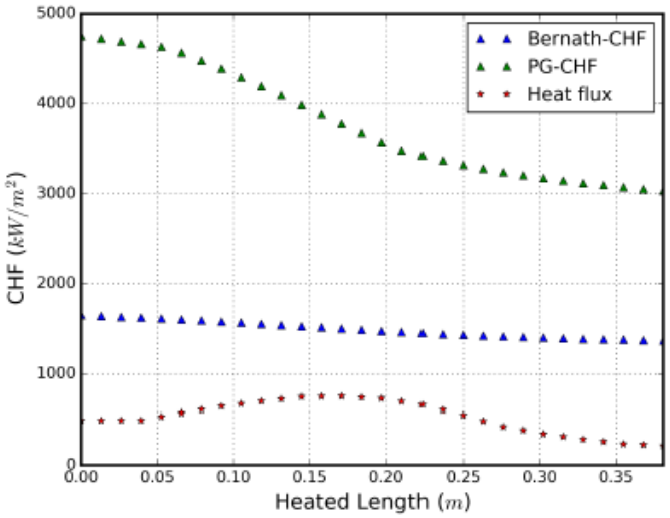

Figure 4.13 - CHF versus heated length

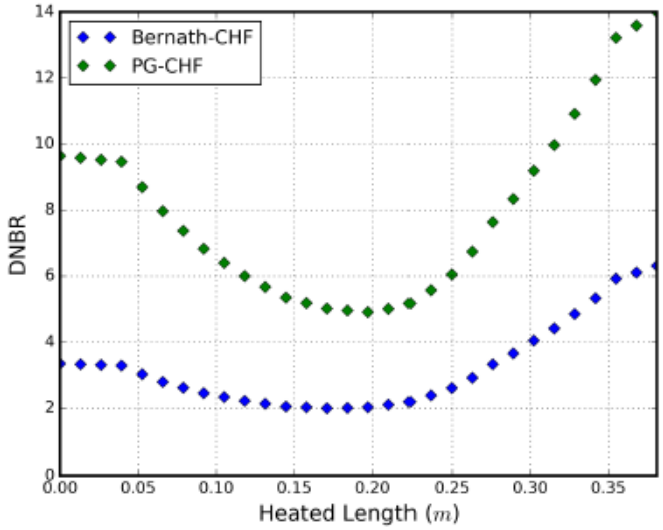

Figure 4.14 - DNBR versus heated length

Formatted: Centered, Keep with next

Formatted: Caption, Centered

Formatted: Centered, Keep with next

Formatted: Caption, Centered

Deleted: Original (12/04)

d. Pulsed Mode of Operation

Transient calculations have been performed using a custom computer code TASCOT for transient and steady state two-dimensional conduction calculations (Ahrens 1999). For these calculations, the initial axial and radial distribution of fuel temperature was based on Eqs. (1) and (3), with the peak fuel temperature set to 746 °C, i.e., a temperature rise of 719 °C above 27 °C ambient temperature. The temperature rise is computed in Chapter 13, Section 13.2.3 for a 2.1% ($3.00) pulse from zero power and a 0.7% ($1.00) pulse from power operation. In the TASCOT calculations, thermal conductivity was set to 0.18 W cm^{-1} K^{-1} (Table 4.1) and the overall heat transfer coefficient U was set to 0.21 W cm^{-1} K^{-1}. The convective heat transfer coefficient was based on the boiling heat transfer coefficient computed using the formulation (Chen 1963, Collier and Thome 1994)

$$q'' = h_b(T_w - T_{sat}) = h(T_w - T_b). \qquad (11)$$

The boiling heat transfer coefficient is given by the correlation (Forster & Zuber 1955)

$$h_b = 0.00122 * \left[\frac{k_f^{0.79} * c_{pf}^{0.45} * \lambda^{0.51}}{\sigma^{0.5} * \mu_f^{0.29} * \rho_g^{0.24} * \left(v_g - v_v\right)^{0.75} * T_{sat}^{0.75}} \right] * \left(T_w - T_{sat}\right)^{0.99}, \qquad (12)$$

in which T_w is the cladding outside temperature, T_{sat} the saturation temperature (111.9 °C), and T_b the coolant ambient temperature (27°C). Fluid-property symbols and values are given in Appendix B. Subscripts f and g refer respectively to liquid and vapor phases. The overall heat transfer coefficient U varies negligibly for ambient temperatures from 20 to 60 °C, and has the value 0.21 W cm^{-1} K^{-1} at T_b = 27 °C.

Figure 4.15 illustrates the radial variation of temperature within the fuel, at the midplane of the core, as a function of time after the pulse. Table 4.10 lists temperatures and heat fluxes as function of time after a 2.1% ($3.00) reactivity insertion in a reactor initially at zero power. The CHFR is based on the critical heat flux of 1.52 MW m^{-2}, the CHF corresponding to the maximum heat flux observed in the axial direction (see Figure 4.13). Figure 4A.3 of Appendix A, using the Ellion data, indicates a Leidenfrost temperature in excess of 500°C. Thus transition boiling, but not fully developed film boiling might be expected for a short time after the end of a pulse.

Formatted: Font:11 pt, Not Bold

Formatted: Justified, Don't adjust space between Latin and Asian text, Don't adjust space between Asian text and numbers

Deleted: temperature

Deleted: 6

Deleted: 9

Deleted: 7

Deleted: 10

Deleted: 8

Deleted: 9

Deleted: 9

Deleted: 10

Deleted: 4

Deleted: 8

Deleted: 49

Deleted: [1]

Deleted: from Eqs. (3) and (4) and from Table 4.2 for saturated boiling

Deleted: Original (12/04)

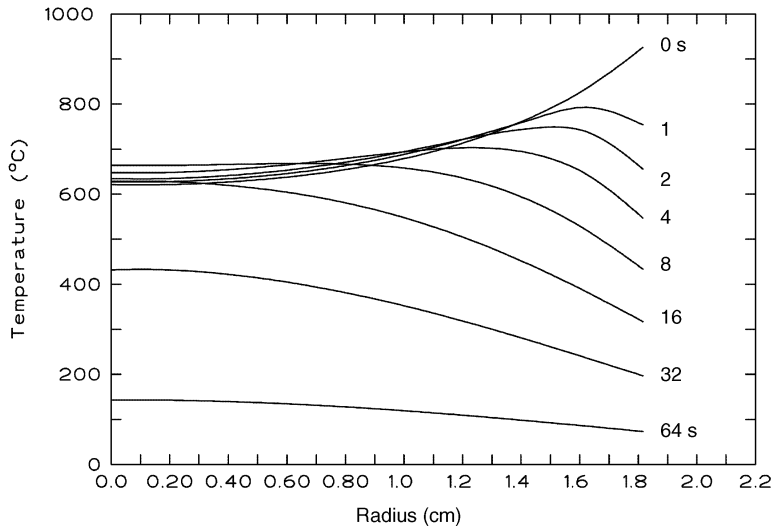

Figure 4.15, Midplane Radial Variation of Temperature Within the Fuel Subsequent to a $3.00 Pulse.

Deleted:

Deleted: 4

Deleted: Original (12/04)

Table 4.10, Heat Flux and Fuel Temperatures Following a $3.00 Pulse from Zero Power, with 27(°C) Coolant Ambient Temperature.

Time (s)	Q'' (W m^{-2})	CHFR	Fuel outside Temp. (°C)	Clad surface Temp. (°C)
0	-	-	953	-
1	3.57×10^5	4.3	781	224
2	7.34×10^5	2.1	683	432
4	8.52×10^5	1.8	574	498
8	7.54×10^5	2.0	461	443
16	5.71×10^5	2.7	344	342
32	3.46×10^5	4.4	224	218
64	1.04×10^5	14.6	100	84

Deleted: 2
Deleted: 0
Deleted: 7
Deleted: 6
Deleted: 3
Deleted: 4

4.6 Thermal Hydraulic Design and Analysis

A balance between the buoyancy driven pressure gain and the frictional and acceleration pressure losses accrued by the coolant in its passage through the core determines the coolant mass flow rate through the core, and the corresponding coolant temperature rise. The buoyancy pressure gain is given by

$$\Delta p_g = \rho_o \beta_o \Delta T g L, \qquad (13)$$

Deleted: 10
Deleted: 11

in which ρ_o and β_o are the density and volumetric expansion coefficient at core inlet conditions (27°C, 0.15285 Mpa), g is the acceleration of gravity, 9.8 cm^2 s^{-1}, ΔT is the temperature rise through the core, and L is the height of the core (between gridplates), namely, 0.556 m. The frictional pressure loss is given by

$$\Delta p_f = \frac{\dot{m}^2 f L}{2 A^2 D_h \rho_o}, \qquad (14)$$

Deleted: 11
Deleted: 12

in which $\dot{m}$ is the coolant mass flow rate (kg s^{-1}) in a unit cell approximated as the equivalent annulus surrounding a single fuel element, A is the flow area, namely, 0.00062 m^2, and D_h is the hydraulic diameter, namely, 0.02127 m. The friction factor f for laminar flow through the annular area is given by 100 Re^{-1} (Shah & London 1978), in which the Reynolds number is given by $D_h \dot{m} / A \mu_o$ in which μ_o is the dynamic viscosity at core inlet conditions.

Entrance of coolant into the core is from the side, above the lower grid plate (see Section 4.2.5), and the entrance pressure loss would be expected to be negligible. The exit contraction loss is given by

$$\Delta p_e = \frac{\dot{m}^2 K}{2 \rho_o A^2}. \qquad (15)$$

Deleted: 12
Deleted: 13

Deleted: Original (12/04)

The coefficient K is calculated from geometry of an equilateral-triangle spacer in a circular opening, for which

$$K \cong \left[\frac{A_t}{A_c}\right]^2 = \left[\frac{3 * R^2 \sin 60^o \cos 60^o}{\pi * R^2}\right] = 0.171, \quad (16)$$

where R is the radius of the opening in the upper grid plate. Equations (14) through (16), solved simultaneously yield the mass flow rates per fuel element, and coolant temperature rises through the core listed in Table 4.11.

Table 4.11, Coolant Flow Rate and Temperature Rise for Natural-Convection Cooling the TRIGA Reactor During Steady-State Operations.

P (kWt)	$\dot{m}$ (kg s^{-1})	ΔT (°C)
50	0.047	3.1
100	0.061	4.7
200	0.077	7.5
300	0.090	9.6
400	0.100	11.5
500	0.108	13.3
750	0.125	17.2
1000	0.139	20.6
1250	0.150	23.8

4.7 Safety Limit

As described in 3.5.1 (Fuel System) and NUREG 1282, fuel temperature limits both steady-state and pulse-mode operation. The fuel temperature limit stems from potential hydrogen outgassing from the fuel and the subsequent stress produced in the fuel element clad material by heated hydrogen gas. Yield strength of cladding material decreases at a temperature of 500°C; consequently, limits on fuel temperature change for cladding temperatures greater than 500°C. A maximum temperature of 1150°C (with clad < 500°C) and 950°C (with clad > 500°C) for U-ZrH ($H/Zr_{1.65}$) will limit internal fuel cladding stresses that might lead to clad integrity (NUREG 1282) challenges.

4.8 Operating Limits

4.8.1 Operating Parameters

The main safety consideration is to maintain the fuel temperature below the value that would result in fuel damage. Setting limits on other operating parameters, that is, limiting safety system settings, controls the fuel temperature. The operating parameters established for the KSU TRIGA reactor are:

Deleted: 13
Deleted: 14
Deleted: 11
Deleted: 12
Deleted: 13
Deleted: 14
Deleted: 9
Deleted: Original (12/04)

- Steady-state power level
- Fuel temperature measured by thermocouple during pulsing operations
- Maximum step reactivity insertion of transient rod

4.8.2 Limiting Safety System Settings

Heat transfer characteristics (from the fuel to the pool) controls fuel temperature during normal operations. As long as thermal hydraulic conditions do not cause critical heat flux to be exceeded, fuel temperature remains well below any limiting value. Figure 4.13 illustrates that critical heat flux is not reached over a wide range of pool temperatures and power levels. As indicated in Figure 4.14, the ratio of actual to critical heat flux is at least 2.0 for temperatures less than 100°C bulk pool water temperature for 1.25 MW operation. Operation at less than 1.25 MW ensures fuel temperature limits are not exceeded by a wide margin.

Deleted: Table 4.9

Limits on the maximum excess reactivity assure that operations during pulsing do not produce a power level (and generate the amount of energy) that would cause fuel-cladding temperature to exceed these limits; no other safety limit is required for pulsed operation.

4.8.3 Safety Margins

For 1,250 kWth steady-state operations, the critical heat flux ratio remains above 2.0 for a core with 85 fuel elements and a maximum radial power peaking factor of 1.63 assuming a coolant inlet temperature of 49°C. The proposed Technical Specifications limit of 44°C on pool inlet temperature ensures that the DNBR will be at least 2.0 during steady-state operation. Limiting pool inlet water temperature to no greater than 44°C (or 37°C with an experiment installed in an interstitial flux-wire port) will ensure that the pool water does not reach temperatures associated with excessive amounts of nucleate boiling.

Deleted: For 1,250 kW steady-state operations, the critical heat flux ratio indicated in Table 4.9 ranges from 5.8 for pool water at room temperature (27°C) to 4.1 at 60 °C (pool temperatures are controlled to less than 48°C for operational concerns). Even at pool water temperatures approaching boiling, the margin remains above 2. Therefore, margins to conditions that could cause excessive temperatures during steady state operations while cladding temperatures is below 500°C are extremely large.

Normal pulsed operations initiated from power levels below 10 kW with a $3.00 reactivity insertion result in maximum hot spot temperatures of 746°C, a 34% margin to the fuel temperature limit. As indicated in Chapter 13, pulsed reactivity insertions of $3.00 from initial conditions of power operation can result in a maximum hot spot temperature of 869°C. Although administratively controlled and limited by an interlock, this pulse would still result in a 15% margin to the fuel temperature safety limit for cladding temperatures below 500°C.

Analysis shows that cladding temperatures will remain below 500°C when fuel is in water except following large pulses. However, mechanisms that can cause cladding temperature to achieve 500°C (invoking a 950°C fuel temperature limit) automatically limit fuel temperature as heat is transferred from the fuel to the cladding.

Immediately following a maximum pulsed reactivity additions, heat transfer driven by fuel temperature can cause cladding temperature to rise above 500°C, but the heat transfer simultaneously cools the fuel to much less than 950°C.

Deleted: Original (12/04)

If fuel rods are placed in an air environment immediately following long-term, high power operation, cladding temperature can essentially equilibrate with fuel temperature. In worst-case air-cooling scenarios, cladding temperature can exceed 500°C, but fuel temperature is significantly lower than the temperature limit for cladding temperatures greater than 500°C.

4.9 Bibliography

"TASCOT: A 2-D, Transient and Steady State Conduction Code for Analyhsis of a TRIGA Fuel Element," Report KSUNE-99-02, Department of Mechanical and Nuclear Engineering, Kansas State University, Manhattan, Kansas, 1999. Ahrens, C.,

"Investigation of the Radial Variation of the Fission-Heat Source in a TRIGA Mark III Fuel Element Using MCNP," Report KSUNE-99-01, Department of Mechanical and Nuclear Engineering, Kansas State University, Manhattan, Kansas, 1999a. Ahrens, C.,

"A Theory of Local Boiling Burnout and Its Application to Existing Data," Heat Transfer - Chemical Engineering Progress Symposium Series, Storrs, Connecticut, 1960, v. 56, No. 20. Bernath, L.,

"A Correlation for Boiling Heat Transfer to Saturated Fluids in Convective Flow," ASME Preprint 63-HT-34, 6th National Heat Transfer Conference, Boston, 1963. Chen, J.C.,

"*Fundamental approach to TRIGA steady-state thermal-hydraulic CHF analysis,"* Technical report, Argonne National Laboratory, 2008, E.E. Feldman.

Kansas State University TRIGA MkII Reactor Hazards Summary Report," License R-88, Docket 50-188, 1961. Clack, R.W., J.R. Fagan, W.R. Kimel, and S.Z. Mikhail

Convective Boiling and Condensation, 3rd ed., Oxford Press, New York, 1994.Collier, J.G., and J.R. Thome,

"Bubble Dynamics and Boiling Heat Transfer," **AIChE Journal 1**, 532 (1955). Forster, H.K., and N. Zuber,

Theory and Design of Modern Pressure Vessels, 2d. ed., Van Nostrand Reinhold, New York, 1974. p. 32. Harvey, J.F.,

"On the Relevance of the Vapour-Liquid Exchange Mechanism for Sub-Cooled Boiling Heat Transfer at High Pressure." Report AEEW-R-137, United Kingdom Atomic Energy Authority, Winfrith, 1978. Ivey, H. J. and D. J. Morris

"On the prediction of the Minimum pool boiling heat flux," J. Heat Transfer, Trans. ASME, 102, 457-460 (1980). Lienhard, J. H. and V. K. Dhir,

Thermal Migration of Hydrogen in Uranium-Zirconium Alloys, General Dynamics, General Atomic Division Report GA-3618, November 1962. Merten, U., et al.,

Deleted: Original (12/04)

MNRC, McClellan Nuclear Radiation Center Facility Safety Analysis Report, Rev. 2, April 1998.

NUREG-1282, "Safety Evaluation Report on High-Uranium Content, Low-Enriched Uranium-Zirconium Hydride Fuels for TRIGA Reactors," U.S. Nuclear Regulatory Commission, 1987.

RELAP5/mod3.3 Code Manual Volume 1: Code structure, system models, and solution methods.

"Laminar Forced Convection in Ducts," p. 357, Academic Press, New York, 1978. Shah, R.K., and A.L. London,

"The U-Zr-Hx Alloy: Its Properties and Use in TRIGA Fuel," Report E-117-833, General Atomics Corp., 1980. Simnad, M.T.

"Safety Analysis Report, TRIGA Reactor Facility, Nuclear Engineering Teaching Laboratory, University of Texas at Austin, Revision 1.01, Docket 50-602, May, 1991.

"*Prediction of departure from nucleate boiling for an axially non-uniform heat flux distribution.*" **Journal of Nuclear Energy 21** (3): 241-248, 1967, L.S. Tong.

Formatted: Normal, Don't adjust space between Latin and Asian text, Don't adjust space between Asian text and numbers

Deleted: Original (12/04)

Appendix 4-A
Post-Pulse Fuel and Cladding Temperature

This discussion is reproduced from Safety Analysis Reports for the University of Texas Reactor Facility (UTA 1991) and the McClellan Nuclear Radiation Center (MNRC 1998).

The following discussion relates the element clad temperature and the maximum fuel temperature during a short time after a pulse. The radial temperature distribution in the fuel element immediately following a pulse is very similar to the power distribution shown in Figure 4A.1. This initial steep thermal gradient at the fuel surface results in some heat transfer during the time of the pulse so that the true peak temperature does not quite reach the adiabatic peak temperature. A large temperature gradient is also impressed upon the clad which can result in a high heat flux from the clad into the water. If the heat flux is sufficiently high, film boiling may occur and form an insulating jacket of steam around the fuel elements permitting the clad temperature to tend to approach the fuel temperature. Evidence has been obtained experimentally which shows that film boiling has occurred occasionally for some fuel elements in the Advanced TRIGA Prototype Reactor located at GA Technologies [Coffer 1964]. The consequence of this film boiling was discoloration of the clad surface.

Thermal transient calculations were made using the RAT computer code. RAT is a 2-D transient heat transport code developed to account for fluid flow and temperature dependent material properties. Calculations show that if film boiling occurs after a pulse it may take place either at the time of maximum heat flux from the clad, before the bulk temperature of the coolant has changed appreciably, or it may take place at a much later time when the bulk temperature of the coolant has approached the saturation temperature, resulting in a markedly reduced threshold for film boiling. Data obtained by Johnson et al. [1961] for transient heating of ribbons in 100°F water, showed burnout fluxes of 0.9 to 2.0 Mbtu ft^{-2} hr^{-1} for e-folding periods from 5 to 90 milliseconds. On the other hand, sufficient bulk heating of the coolant channel between fuel elements can take place in several tenths of a second to lower the departure from nucleate boiling (DNB) point to approximately 0.4 Mbtu ft^{-2} hr^{-1}. It is shown, on the basis of the following analysis, that the second mode is the most likely; i.e., when film boiling occurs it takes place under essentially steady-state conditions at local water temperatures near saturation.

A value for the temperature that may be reached by the clad if film boiling occurs was obtained in the following manner. A transient thermal calculation was performed using the radial and axial power distributions in Figures 4A.1and 4A.2, respectively, under the assumption that the thermal resistance at the fuel-clad interface was nonexistent. A boiling heat transfer model, as shown in Figure 4A.3, was used in order to obtain an upper limit for the clad temperature rise. The model used the data of McAdams [1954] for subcooled boiling and the work of Sparrow and Cess [1962] for the film boiling regime. A conservative estimate was obtained for the minimum heat flux in film boiling by using the correlations of Speigler et al. [1963], Zuber [1959], and Rohsenow and Choi [1961] to find the minimum temperature point at which film boiling could occur. This calculation gave an upper limit of 760°C clad temperature for a peak initial fuel temperature of 1000°C, as shown in Figure. 4A.4. Fuel temperature distributions for this case are shown in Figure 4A.5 and the heat flux into the water from the clad is shown in Figure 4A.6. In this limiting case, DNB occurred only 13 milliseconds after the pulse, conservatively calculated

Deleted: 6

Deleted: Original (9/02)

assuming a steady-state DNB correlation. Subsequently, experimental transition and film boiling data were found to have been reported by Ellion [9] for water conditions similar to those for the TRIGA system. The Ellion data show the minimum heat flux, used in the limiting calculation described above, was conservative by a factor of 5. An appropriate correction was made which resulted in a more realistic estimate of 470°C as the maximum clad temperature expected if film boiling occurs. This result is in agreement with experimental evidence obtained for clad temperatures of 400°C to 500°C for TRIGA Mark F fuel elements which have been operated under film boiling conditions [Coffer et al. 1965].

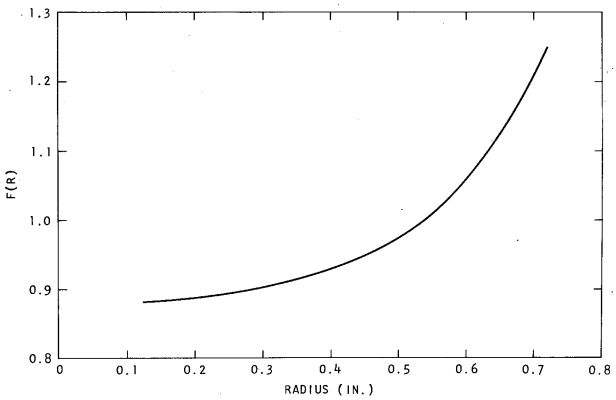

Figure 4A.1. Representative Radial Variation of Power Within the TRIGA Fuel Rod

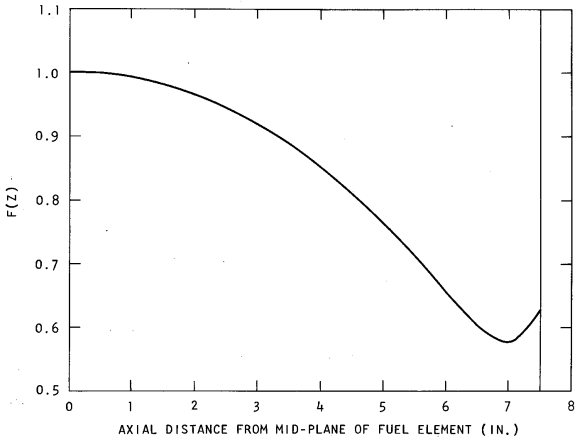

Figure 4A.2, Representative Axial Variation of Power Within the TRIGA Fuel Rod.

Deleted: 6

Deleted: Original (9/02)

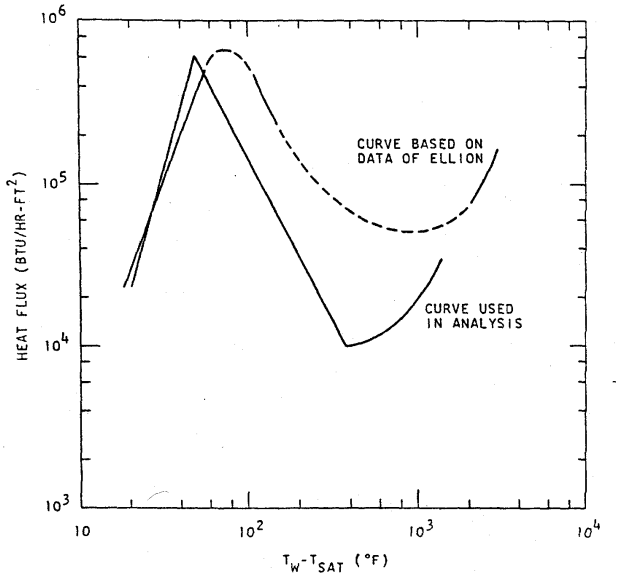

Figure 4A.3, Subcooled Boiling Heat Transfer for Water.

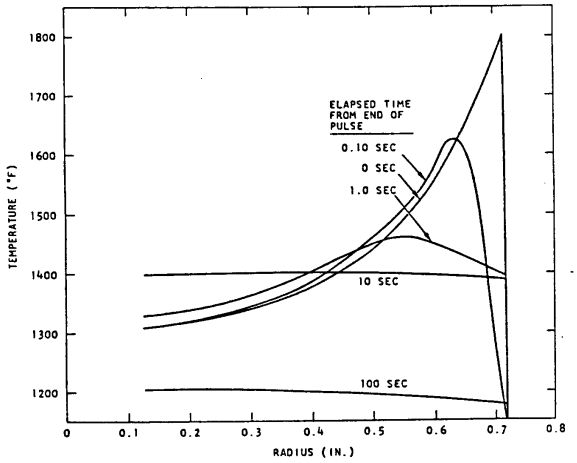

Figure 4A.4, Fuel Body Temperature at the Midplane of a Well-Bonded Fuel Element After Pulse.

Deleted: 6

Deleted: Original (9/02)

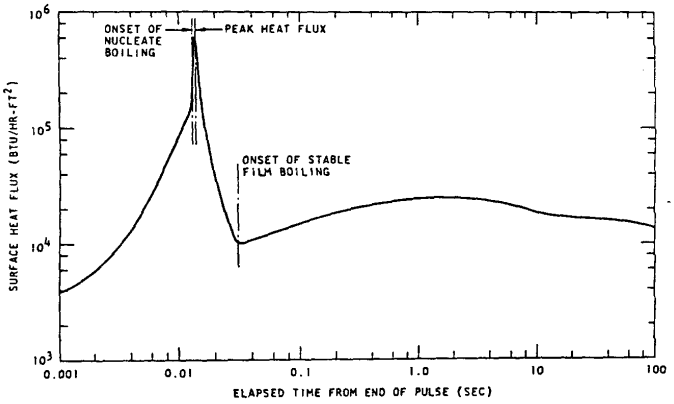

Figure 4A.5, Surface Heat Flux at the Midplane of a Well Bonded Fuel Element After a Pulse.

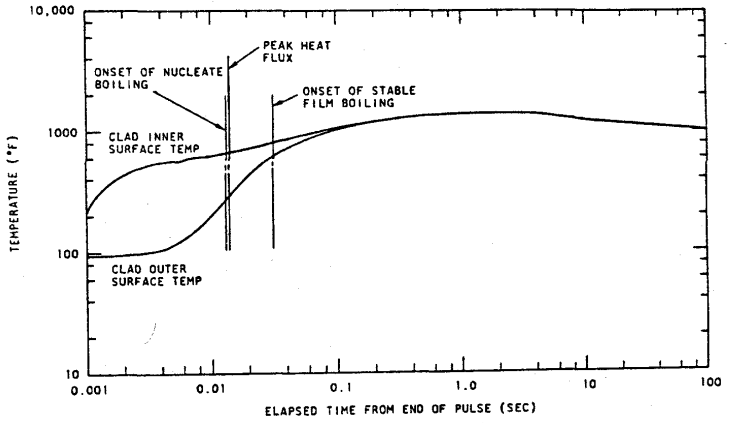

Figure 4A.6, Clad Temperature at Midpoint of Well-Bonded Fuel Element.

Deleted: 6

Deleted: Original (9/02)

The preceding analysis assessing the maximum clad temperatures associated with film boiling

assumed no thermal resistance at fuel-clad interface. Measurements of fuel temperatures as a function of steady-state power level provide evidence that after operating at high fuel temperatures, a permanent gap is produced between the fuel body and the clad by fuel expansion. This gap exists at all temperatures below the maximum operating temperature. (See, for example, Figure 16 in the Coffer report [1965].) The gap thickness varies with fuel temperature and clad temperature so that cooling of the fuel or overheating of the clad tends to widen the gap and decrease the heat transfer rate. Additional thermal resistance due to oxide and other films on the fuel and clad surfaces is expected. Experimental and theoretical studies of thermal contact resistance have been reported [Fenech and Rohsenow 1959, Graff 1960, Fenech and Henry 1962] which provide insight into the mechanisms involved. They do not, however, permit quantitative prediction of this application because the basic data required for input are presently not fully known. Instead, several transient thermal computations were made using the RAT code. Each of these was made with an assumed value for the effective gap conductance, in order to determine the effective gap coefficient for which departure from nucleate boiling is incipient. These results were then compared with the incipient film boiling conditions of the 1000°C peak fuel temperature case.

For convenience, the calculations were made using the same initial temperature distribution as was used for the preceding calculation. The calculations assumed a coolant flow velocity of 1 ft per second, which is within the range of flow velocities computed for natural convection under various steady-state conditions for these reactors. The calculations did not use a complete boiling curve heat transfer model, but instead, included a convection cooled region (no boiling) and a subcooled nucleate boiling region without employing an upper DNB limit. The results were analyzed by inspection using the extended steady-state correlation of Bernath [1960] which has been reported by Spano [1964] to give agreement with SPERT II burnout results within the experimental uncertainties in flow rate.

The transient thermal calculations were performed using effective gap conductances of 500, 375, and 250 Btu ft^{-2} hr^{-1} $°F^{-1}$. The resulting wall temperature distributions were inspected to determine the axial wall position and time after the pulse which gave the closest approach between the local computed surface heat flux and the DNB heat flux according to Bernath. The axial distribution of the computed and critical heat fluxes for each of the three cases at the time of closest approach is given in Figures 4A.7 through 4A.9. If the minimum approach to DNB is corrected to TRIGA Mark F conditions and cross-plotted, an estimate of the effective gap conductance of 450 Btu ft^{-2} hr^{-1} $°F^{-1}$ is obtained for incipient burnout so that the case using 500 is thought to be representative of standard TRIGA fuel.

The surface heat flux at the midplane of the element is shown in Figure 4A.10 with gap conductance as a parameter. It may be observed that the maximum heat flux is approximately proportional to the heat transfer coefficient of the gap, and the time lag after the pulse for which the peak occurs is also increased by about the same factor. The closest approach to DNB in these calculations did not necessarily occur at these times and places, however, as indicated on the curves of Figures 4A.7 through 4A.9. The initial DNB point occurred near the core outlet for a local heat flux of about 340 kBtu ft^{-2} hr^{-1} $°F^{-1}$ according to the more conservative Bernath correlation at a local water temperature approaching saturation.

Deleted: 6

Deleted: Original (9/02)

This analysis indicates that after operation of the reactor at steady-state power levels of 1 MW(t), or after pulsing to equivalent fuel temperatures, the heat flux through the clad is reduced and therefore reduces the likelihood of reaching a regime where there is a departure from nucleate boiling. From the foregoing analysis, a maximum temperature for the clad during a pulse which gives a peak adiabatic fuel temperature of 1000°C is conservatively estimated to be 470°C.

As can be seen from Figure 4.7, the ultimate strength of the clad at a temperature of 470°C is 59,000 psi. If the stress produced by the hydrogen over pressure in the can is less than 59,000 psi, the fuel element will not undergo loss of containment. Referring to Figure 4.8, and considering U-ZrH fuel with a peak temperature of 1000°C, one finds the stress on the clad to be 12,600 psi. Further studies show that the hydrogen pressure that would result from a transient for which the peak fuel temperature is 1150°C would not produce a stress in the clad in excess of its ultimate strength. TRIGA fuel with a hydrogen to zirconium ratio of at least 1.65 has been pulsed to temperatures of about 1150°C without damage to the clad [Dee et al. 1966].

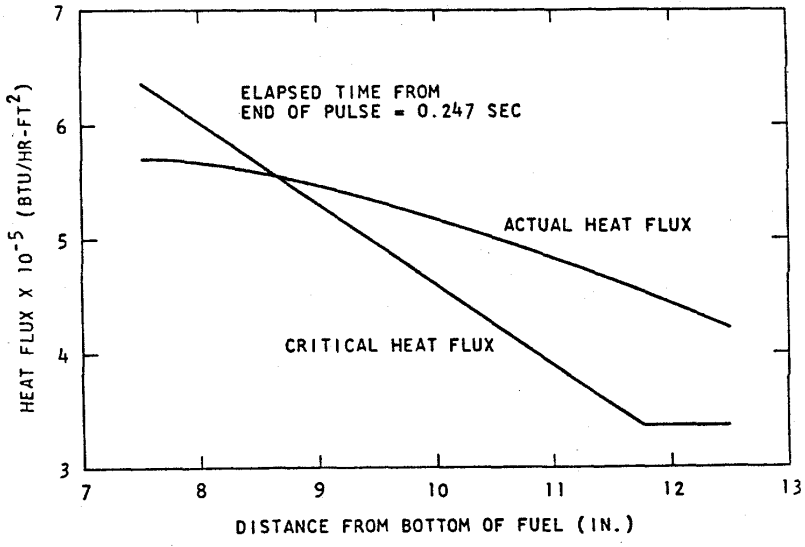

Figure 4A.7, Surface Heat Flux Distribution for Standard Non-Gapped (h_{gap} = 500 Btu/h ft^2 ^{o}F) Fuel Element After a Pulse.

Deleted: .

Deleted: 6

Deleted: Original (9/02)

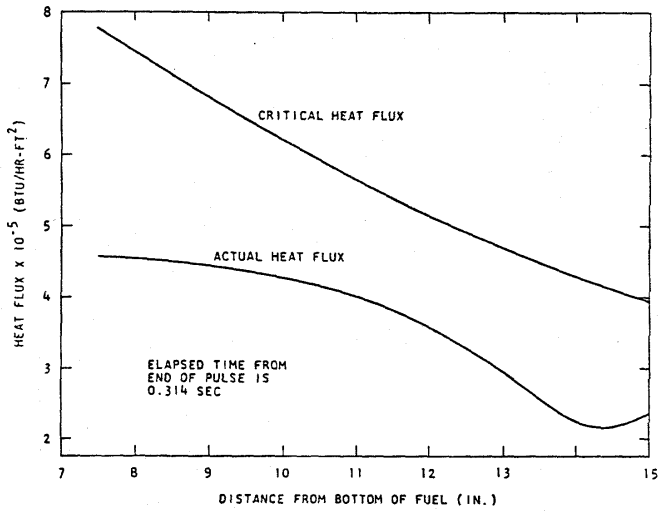

Figure 4A.8, Surface Heat-Flux Distribution for Standard Non-Gapped Fuel Element (h_{gap} = 375 Btu/h ft^2 ^{o}F) After a Pulse.

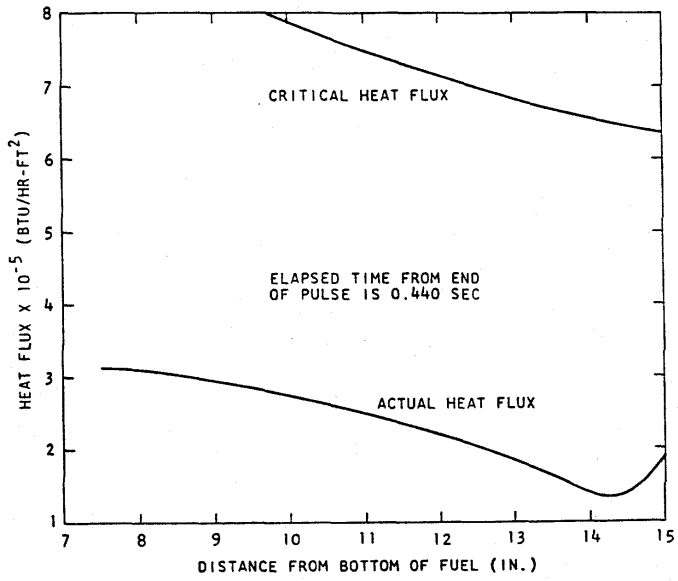

Figure 4A.9, Surface Heat-Flux Distribution for Standard Non-Gapped Fuel Element (h_{gap} = 250 Btu/h ft^2 ^{o}F) After a Pulse.

Deleted: 6

Deleted: Original (9/02)

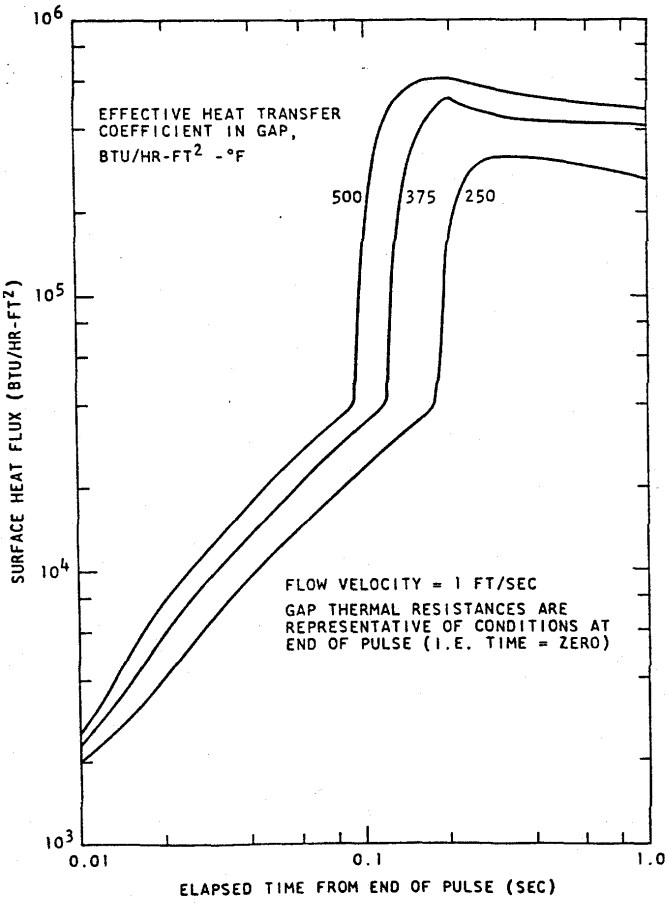

Figure 4A.10, Surface Heat Flux at Midpoint vs. Time for Standard Non-Gapped Fuel Element After a Pulse.

Deleted: 6

Deleted: Original (9/02)

Bibliography

"A Theory of Local Boiling Burnout and Its Application to Existing Data," Heat Transfer - Chemical Engineering Progress Symposium Series, Storrs, Connecticut, 1960, v. 56, No. 20. Bernath, L.,

Research in Improved TRIGA Reactor Performance, Final Report, General Dynamics, General Atomic Division Report GA-5786, October 20, 1964. Coffer, C.O., et al.,

Characteristics of Large Reactivity Insertions in a High Performance TRIGA U-ZrH Core, General Dynamics, General Atomic Division Report GA-6216, April 12, 1965.Coffer, C. O., et al.

Annular Core Pulse Reactor, General Dynamic, General Atomic Division Report GACD 6977, Supplement 2, 1966.Dee, J. B., T. B. Pearson, J. R. Shoptaugh, Jr., M. T. Simnad,

Temperature Variation, Heat Transfer, and Void Volume Development in the Transient Atmosphere Boiling of Water, Report SAN-1001, U. Cal., Berkeley, January, 1961. Johnson, H.A., and V.E. Schrock, et al.,

A Study of the Mechanism of Boiling Heat Transfer, JPL Memorandum No. 20-88, March 1, 1954.Ellion, M.E.,

Thermal Conductance of Metallic Surfaces in Contact, USAEC NYO-2130, May, 1959.Fenech, H., and W. Rohsenow,

An Analysis of a Thermal Contact Resistance, **Trans. ANS 5**, p. 476, 1962.Fenech, H., and J.J. Henry,

"Thermal Conductance Across Metal Joints, " **Machine Design**, Sept. 15, 1960, pp 166-172. Graff, W.J.

Heat Transmission, 3rd Ed., McGraw-Hill, 1954McAdams, -W.H ..

MNRC, McClellan Nuclear Radiation Center Facility Safety Analysis Report, Rev. 2, April 1998.

Heat, Mass and Momentum Transfer, Prentice-Hall, 1961, pp 231-232.Rohsenow, W., and H. Choi,

"Quarterly Technical Report SPERT Project, April, May, June, 1964, " ISO 17030. Spano, A. H.,

"The Effect of Subcooled Liquid on Film Boiling," **Heat Transfer 84**, 149-156, (1962).Sparrow, E.M. and R.D. Cess,

Deleted: "*Fundamental approach to TRIGA steady-state thermal-hydraulic CHF analysis,"* Technical report, Argonne National Laboratory, 2008, E.E. Feldman. ... [42]

Formatted: Normal

Formatted: Font:(Default) Times New Roman, 11 pt

Formatted: Font:(Default) Times New Roman, 11 pt

Deleted:

Formatted: Font:(Default) Times New Roman, 11 pt, Italic

Formatted: Font:(Default) Times New Roman, 11 pt

Formatted: Font:(Default) Times New Roman, 11 pt, Italic

Formatted: Font:(Default) Times New Roman, 11 pt

Formatted: Font:(Default) Times New Roman, 11 pt, Bold

Formatted: Font:(Default) Times New Roman, 11 pt

Deleted: Page Break

Deleted: 6

Deleted: Original (9/02)

"Onset of Stable Film Boiling and the Foam Limit," **Int. J. Heat and Mass Transfer 6**, 987-989, (1963). Speigler, P., et al.,

UTA, University of Texas at Austin TRIGA Reactor Facility Safety Analysis Report, Docket 50-602, Rev. 1.01, May 1991.

"Hydrodynamic Aspects of Boiling Heat Transfer," AEC Report AECV-4439, TIS, ORNL, 1959. Zuber, W.

Deleted: 6

Deleted: Original (9/02)

Appendix B
Water Properties at Nominal Operating Conditions

Data for 16 Feet of Water over the Core

T_{pool} °C	ρ_T[1] kg m^{-3}	$\rho_{f,16}$[1] kg m^{-3}	$P_{h,16}$[2] kPa	$h_{f,16}$[1] kJ kg^{-1}	$h_{g,16}$[1] kJ kg^{-1}	$\rho_{g,16}$[1] kg m^{-3}	$T_{sat,16}$[1] °C	q"$_{sat,16}$[3] W m^{-2}	q"sub[4] W m^{-2}
15	999.21	950.00	47.79	465.10	2692.64	0.85	110.89	1553.842	7239.19
20	998.32	950.01	47.74	465.05	2692.63	0.85	110.88	1552.078	6931.74
25	997.16	950.02	47.69	465.01	2692.59	0.85	110.87	1549.496	6622.60
30	995.75	950.03	47.62	464.95	2692.59	0.85	110.86	1547.118	6311.82
35	994.12	950.04	47.54	464.89	2692.57	0.85	110.84	1543.981	5999.91
40	992.29	950.06	47.46	464.81	2692.54	0.85	110.83	1540.446	5688.24
45	990.27	950.07	47.36	464.73	2692.51	0.85	110.81	1536.512	5376.29
50	988.07	950.09	47.25	464.64	2692.48	0.85	110.78	1532.205	5064.36
55	985.70	950.11	47.14	464.54	2692.45	0.85	110.76	1527.561	4753.90
60	983.18	950.12	47.02	464.44	2692.41	0.85	110.74	1522.575	4444.85
65	980.50	950.14	46.89	464.33	2692.37	0.85	110.71	1517.255	4136.85
70	977.69	950.17	46.76	464.21	2692.33	0.84	110.68	1511.666	3830.73
75	974.74	950.19	46.62	464.09	2692.29	0.84	110.65	1505.778	3526.89
80	971.66	950.21	46.47	463.96	2692.24	0.84	110.62	1499.613	3225.47
85	968.45	950.23	46.32	463.83	2692.19	0.84	110.59	1493.199	2926.81
90	965.12	950.26	46.16	463.69	2692.15	0.84	110.56	1486.527	2631.05
95	961.68	950.29	45.99	463.55	2692.09	0.84	110.53	1479.626	2338.47
97	960.27	950.30	45.92	463.49	2692.07	0.84	110.51	1472.944	2216.11
99	958.84	950.31	45.86	463.43	2692.05	0.84	110.50	1466.058	2095.18

Data for 13 Feet of Water over the Core

T_{pool} °C	ρ_T[1] kg m^{-3}	$\rho_{f,13}$[1] kg m^{-3}	$P_{h,13}$[2] kPa	$h_{f,13}$[1] kJ kg^{-1}	$h_{g,13}$[1] kJ kg^{-1}	$\rho_{g,13}$[1] kg m^{-3}	$T_{sat,13}$[1] °C	q"$_{sat,13}$[3] W m^{-2}	q"sub[4] W m^{-2}
15	999.21	951.43	38.83	457.21	2689.85	0.80	109.03	1513.00	6964.74
20	998.32	951.43	38.79	457.18	2689.84	0.80	109.02	1511.32	6857.12
25	997.16	951.44	38.75	457.13	2689.82	0.80	109.01	1509.15	6543.62
30	995.75	951.45	38.69	457.09	2689.80	0.80	109.00	1505.85	6229.30
35	994.12	951.46	38.63	457.03	2689.78	0.80	108.99	1503.13	5913.58
40	992.29	951.47	38.56	456.96	2689.76	0.80	108.97	1500.16	5597.21
45	990.27	951.49	38.48	456.89	2689.74	0.80	108.96	1496.38	5281.90
50	988.07	951.50	38.39	456.82	2689.71	0.80	108.94	1492.25	4966.66
55	985.70	951.51	38.30	456.73	2689.68	0.80	108.92	1487.78	4652.39
60	983.18	951.53	38.20	456.64	2689.65	0.80	108.90	1482.99	4339.60
65	980.50	951.55	38.10	456.55	2689.61	0.80	108.87	1477.90	4027.94
70	977.69	951.57	37.99	456.45	2689.58	0.80	108.85	1472.52	3718.83
75	974.74	951.58	37.88	456.35	2689.54	0.80	108.83	1466.86	3412.07
80	971.66	951.60	37.76	456.24	2689.50	0.80	108.80	1460.95	3107.29
85	968.45	961.62	37.63	456.12	2689.46	0.80	108.77	1458.59	2812.63
90	965.12	951.64	37.50	456.01	2689.42	0.79	108.75	1448.37	2506.90
95	961.68	951.67	37.37	455.89	2689.38	0.79	108.72	1441.74	2211.19
97	960.27	951.68	37.31	455.84	2689.36	0.79	108.70	1435.27	2087.92
99	958.84	951.68	37.26	455.78	2689.34	0.79	108.69	1428.60	1966.16

Deleted: 6

Deleted: Revised 04/19/17

Common Data

T °C	P_{atm} kPa	c_p[1] kJ kg^{-1} k^{-1}	σ N m^{-1}
15	99.83	4.23080	0.07149
20	99.83	4.23080	0.07120
25	99.83	4.23080	0.07083
30	99.83	4.23080	0.07039
35	99.83	4.23070	0.06989
40	99.83	4.23070	0.06932
45	99.83	4.23070	0.06869
50	99.83	4.23070	0.06800
55	99.83	4.23060	0.06727
60	99.83	4.23060	0.06649
65	99.83	4.23060	0.06566
70	99.83	4.23050	0.06480
75	99.83	4.23050	0.06390
80	99.83	4.23050	0.06297
85	99.83	4.23040	0.06201
90	99.83	4.23040	0.06102
95	99.83	4.23040	0.06001
97	99.83	4.23030	0.05898
99	99.83	4.23030	0.05793

NOTE[1]: 1967 ASME (IFC) Steam Tables & IAPWS-IF97

*NOTE[2]:kPa =Heigth(ft)*12(in/ft)*0.0254(meters/in)*Density(kg/m^3)*9.80665/1000*

NOTE[3]: $q''_{SAT} = 0.149 \cdot \rho_g{}^{0.5} \cdot \left(h_{g,sat} - h_{f,sat}\right) \cdot \left(\cdot\, g \cdot \sigma \cdot \left\{\rho_f - \rho_g\right\}\right)^{1/4}$

NOTE[4]: $q''_{sub} = q''_{SAT} \cdot \left(1 + 0.1 \cdot \left(\frac{\rho_f}{\rho_g}\right)^{3/4} \cdot \frac{c_{p,f} \cdot \left(T_{SAT} - T_{sub}\right)}{h_{g,sat} - h_{f,sat}}\right)$

NOTE:[5]:

$\sigma = 1.000\text{E-}11 \cdot T^4 + 7.370\text{E-}09 \cdot T^3 - 1.969\text{E-}06 \cdot T^2 + 4.709\text{E-}06 \cdot T + 7.1833\text{E-}02$

Deleted: A-12

Deleted: 6

Deleted: Original (9/02)

The margin to critical heat flux for the reference core was determined. Critical heat flux for saturated pool boiling is given by (***Heat Transfer***, A. Bejan, 1993, John Wiley & Sons):

$$q''_{SAT} = 0.149 \cdot \rho_g^{0.5} \cdot \left(h_{g,sat} - h_{f,sat}\right) \cdot \left(g \cdot \sigma \cdot \left\{\rho_f - \rho_g\right\}\right)^{1/4} \quad (3)$$

where ρ_f is the density of the fluid, ρ_g is the density of the vapor, σ is the surface tension of the liquid phase in contact with vapor, $h_{f,sat}$ is the enthalpy of the saturated fluid, and $h_{g,sat}$ is the enthalpy of the vapor phase with all values at saturation conditions of temperature and pressure. Surface tension data provided by Bejan was fit to a polynomial (using temperature in ºC) to generate data for the temperature range of interest, with an R^2 value of 0.999998:

$$\sigma = 1.000\text{E-}11 \cdot T^4 + 7.370\text{E-}09 \cdot T^3 - 1.969\text{E-}06 \cdot T^2 + 4.709\text{E-}06 \cdot T + 7.1833\text{E-}02$$

Pressure at the core is determined by barometric pressure at the facility elevation, vacuum maintained in the reactor bay and the weight of the water over the core. Barometric pressure associated with the Manhattan, Kansas airport is 29.92 in. Hg. The reactor bay is maintained at a slight vacuum, with the maximum gage pressure (6 in, of water) corresponding to -0.44 in Hg; nominal barometric pressure corrected for maximum reactor bay vacuum (a change of approximately 1.5%) corresponds to 99.83 kPa. Variations in local barometric pressure are on the order of the correction for reactor bay pressure or less, so that the variations can be neglected without significant error. Normal pool level provides 16 feet of water over the core, contributing a nominal static pressure of 47.83 kPa. A pool level of 13 feet contributes a nominal static pressure of 38.58 kPa. (Vacuum breakers are installed in the cooling system piping about 3 feet below the surface of the pool water to limit potential siphoning of the pool.) Actual hydrostatic pressure of the pool water above the core is also determined by water density. With reactor bay atmospheric pressure at 99.827 kPa, water boils at 99.85ºC. Therefore, values of thermodynamic properties as tabulated in Chapter 4 Appendix B were determined from the 1967 ASME (IFC) Steam Tables & IAPWS-IF97 with temperatures ranging from a maximum of 99ºC to 15ºC for pressures corresponding to 13 feet and 16 feet of water in the reactor pool.

For subcooled boiling, the critical heat flux is calculated by (Ivey and Morris 1978):

$$q''_{sub} = q''_{SAT} \cdot \left(1 + 0.1 \cdot \left(\frac{\rho_f}{\rho_g}\right)^{3/4} \cdot \frac{c_{p,f} \cdot \left(T_{SAT} - T_{sub}\right)}{h_{g,sat} - h_{f,sat}}\right), \quad (4)$$

where T_{sub} and $c_{p,f}$ correspond to the subcooled fluid. Specific heat capacities at the subcooled fluid temperatures and pressures evaluated above were determined from the 1967 ASME (IFC) Steam Tables & IAPWS-IF97 for the range of interest, as tabulated in Chapter 4 Appendix B. Critical heat flux calculations were compared to the actual heat flux previously calculated to determine the margin as a critical heat flux ratio (CHFR), provided below in Table 4.9.

Table 4.9, Critical Heat Flux Ratios (CHF versus Maximum Heat Flux) for 13 & 16 Feet of Water Over the Core

TEMP	CHFR (13 ft)	CHFR (16 ft)	AVE	Δ/AVE
15	6.58	6.84	6.71	3.86%
20	6.48	6.55	6.51	1.08%
25	6.18	6.26	6.22	1.20%

Table 4.9, Critical Heat Flux Ratios (CHF versus Maximum Heat Flux) for 13 & 16 Feet of Water Over the Core

TEMP	CHFR (13 ft)	CHFR (16 ft)	AVE	Δ/AVE
30	5.88	5.96	5.92	1.32%
35	5.59	5.67	5.63	1.45%
40	5.29	5.37	5.33	1.61%
45	4.99	5.08	5.03	1.77%
50	4.69	4.78	4.74	1.95%
55	4.39	4.49	4.44	2.16%
60	4.10	4.20	4.15	2.40%
65	3.80	3.91	3.86	2.67%
70	3.51	3.62	3.57	2.96%
75	3.22	3.33	3.28	3.31%
80	2.94	3.05	2.99	3.73%
85	2.66	2.76	2.71	3.98%
90	2.37	2.49	2.43	4.83%
95	2.09	2.21	2.15	5.60%
97	1.97	2.09	2.03	5.96%
99	1.86	1.98	1.92	6.35%

As indicated in Table 4.9, the actual heat flux is less than the critical heat flux for operating temperatures up to 55 ºC by more than a factor of 4 considering both 13 feet and 16 feet of water above the core. The CHFR is greater than 2 for pool temperatures exceeding the maximum operating value up to 95 ºC, and remains near 2 at values up to 99ºC. The difference in the critical heat flux ratio for 13 and 16 feet of water is relatively small, with a minimum difference compared to the mean of the two values of 1.8% and a maximum of 3.86% below 60 ºC, 6.4% across all pool temperatures considered.

It is clear from the table that there is a very wide margin between the operating heat flux and the critical heat flux even to unrealistically high pool water temperature, so that film boiling and excessive cladding temperature is not a consideration in steady-state operation.

Page 22: [2] Formatted **Jeffrey Geuther** **4/19/17 4:28:00 PM**

Justified, Don't adjust space between Latin and Asian text, Don't adjust space between Asian text and numbers

Page 22: [3] Formatted **Jeffrey Geuther** **4/19/17 4:24:00 PM**

Font:(Default) Times New Roman, 11 pt

Page 22: [4] Formatted **Jeffrey Geuther** **4/19/17 4:24:00 PM**

Font:(Default) Times New Roman, 11 pt

Page 22: [5] Formatted **Jeffrey Geuther** **4/19/17 4:24:00 PM**

Font:(Default) Times New Roman, 11 pt

Page 22: [6] Formatted **Jeffrey Geuther** **4/19/17 4:24:00 PM**

Font:(Default) Times New Roman, 11 pt

Page 22: [7] Formatted **Jeffrey Geuther** **4/19/17 4:24:00 PM**

Font:(Default) Times New Roman, 11 pt

Page 22: [8] Formatted **Jeffrey Geuther** **4/19/17 4:24:00 PM**

Font:(Default) Times New Roman, 11 pt

Page 22: [9] Formatted	**Jeffrey Geuther**	**4/19/17 4:24:00 PM**

Font:(Default) Times New Roman, 11 pt

Page 22: [10] Formatted	**Jeffrey Geuther**	**4/19/17 4:24:00 PM**

Font:(Default) Times New Roman, 11 pt

Page 22: [11] Formatted	**Jeffrey Geuther**	**4/19/17 4:24:00 PM**

Font:(Default) Times New Roman, 11 pt

Page 22: [12] Formatted	**Jeffrey Geuther**	**4/19/17 4:24:00 PM**

Font:(Default) Times New Roman, 11 pt

Page 22: [13] Formatted	**Jeffrey Geuther**	**4/19/17 4:24:00 PM**

Font:(Default) Times New Roman, 11 pt

Page 22: [14] Formatted	**Jeffrey Geuther**	**4/19/17 4:24:00 PM**

Font:(Default) Times New Roman, 11 pt

Page 22: [15] Formatted	**Jeffrey Geuther**	**4/19/17 4:24:00 PM**

Font:(Default) Times New Roman, 11 pt

Page 22: [16] Formatted	**Jeffrey Geuther**	**4/19/17 4:24:00 PM**

Font:(Default) Times New Roman, 11 pt

Page 22: [17] Formatted	**Jeffrey Geuther**	**4/19/17 4:24:00 PM**

Font:(Default) Times New Roman, 11 pt

Page 22: [18] Formatted	**Jeffrey Geuther**	**4/19/17 4:28:00 PM**

Font:(Default) Times New Roman, 11 pt

Page 22: [19] Formatted	**Jeffrey Geuther**	**4/19/17 4:28:00 PM**

Font:(Default) Times New Roman, 11 pt

Page 22: [20] Formatted	**Jeffrey Geuther**	**4/19/17 4:28:00 PM**

Font:(Default) Times New Roman, 11 pt

Page 22: [21] Formatted	**Jeffrey Geuther**	**4/19/17 4:28:00 PM**

Font:(Default) Times New Roman, 11 pt

Page 22: [22] Formatted	**Jeffrey Geuther**	**4/19/17 4:28:00 PM**

Font:(Default) Times New Roman, 11 pt

Page 22: [23] Formatted	**Jeffrey Geuther**	**4/19/17 4:28:00 PM**

Font:(Default) Times New Roman, 11 pt

Page 22: [24] Formatted	**Jeffrey Geuther**	**4/19/17 4:28:00 PM**

Font:(Default) Times New Roman, 11 pt

Page 22: [25] Formatted	**Jeffrey Geuther**	**4/19/17 4:28:00 PM**

Font:(Default) Times New Roman, 11 pt

Page 22: [26] Formatted	**Jeffrey Geuther**	**4/19/17 4:28:00 PM**

Font:(Default) Times New Roman, 11 pt

Page 22: [27] Formatted	**Jeffrey Geuther**	**4/19/17 4:28:00 PM**

Font:(Default) Times New Roman, 11 pt

Page 22: [28] Formatted	**Jeffrey Geuther**	**4/19/17 4:28:00 PM**

Font:(Default) Times New Roman, 11 pt

Page 22: [29] Formatted	**Jeffrey Geuther**	**4/19/17 4:28:00 PM**

Font:(Default) Times New Roman, 11 pt

Page 22: [30] Formatted	**Jeffrey Geuther**	**4/19/17 4:28:00 PM**

Font:(Default) Times New Roman, 11 pt

Page 22: [31] Formatted	**Jeffrey Geuther**	**4/19/17 4:28:00 PM**

Font:(Default) Times New Roman, 11 pt

Page 22: [32] Formatted	**Jeffrey Geuther**	**4/19/17 4:28:00 PM**

Font:(Default) Times New Roman, 11 pt

Page 22: [33] Formatted	**Jeffrey Geuther**	**4/19/17 4:28:00 PM**

Font:(Default) Times New Roman, 11 pt

Page 22: [34] Formatted	**Jeffrey Geuther**	**4/19/17 4:28:00 PM**

Font:(Default) Times New Roman, 11 pt

Page 22: [35] Formatted	**Jeffrey Geuther**	**4/19/17 4:28:00 PM**

Font:(Default) Times New Roman, 11 pt

Page 22: [36] Formatted	**Jeffrey Geuther**	**4/19/17 4:28:00 PM**

Font:(Default) Times New Roman, 11 pt

Page 22: [37] Formatted	**Jeffrey Geuther**	**4/19/17 4:28:00 PM**

Font:(Default) Times New Roman, 11 pt

Page 22: [38] Formatted	**Jeffrey Geuther**	**4/19/17 4:28:00 PM**

Font:(Default) Times New Roman, 11 pt

Page 22: [39] Formatted	**Jeffrey Geuther**	**4/19/17 4:28:00 PM**

Font:(Default) Times New Roman, 11 pt

Page 22: [40] Formatted	**Jeffrey Geuther**	**4/19/17 4:28:00 PM**

Font:(Default) Times New Roman, 11 pt

Page 22: [41] Formatted	**Jeffrey Geuther**	**4/19/17 4:28:00 PM**

Font:(Default) Times New Roman, 11 pt

Page 9: [42] Deleted	**Amir Bahadori**	**6/27/17 9:04:00 AM**

"*Fundamental approach to TRIGA steady-state thermal-hydraulic CHF analysis,"* Technical report, Argonne National Laboratory, 2008, E.E. Feldman.

RELAP5/mod3.3 Code Manual Volume 1: Code structure, system models, and solution methods.

"*Prediction of departure from nucleate boiling for an axially non-uniform heat ux distribution*." **Journal of Nuclear Energy 21** (3): 241-248, 1967, L.S. Tong.